Ocean Colour

Standard Atmospheric Correction

Product Validation and evolution Report

Deliverable D-5

Version 3.0

29-09-2022

Study funded by EUMETSAT contract EUM/CO/21/4600002533/DD

TABLE OF CONTENTS

1 INTRODUCTION

1.1 SCOPE OF THE DOCUMENT

This document is the Product Validation and evolution Report (PVR) of the EUMETSAT Ocean Colour Standard Atmospheric Correction (OC-SAC) study and constitutes the study deliverable D-5.

This version, 32, is based on the first release of the OC-SAC processor to EUMETSAT (ATBD v4, see [AD-3]). Further tuning and improvements of the processor are foreseen in the future.

1.2 STRUCTURE OF THE DOCUMENT

Present PVR is structured as follows:

- Section 1 describes the structure and applicable documents,
- Section 2 describes the version and configuration of the evaluated products (IPF, OC-SAC),
- Section 3 provides the validation of each product using in-situ data,
- Section 4 provides visualization of sample scenes,
- Section 5 provides global Level-3 maps, and differences maps,
- Section 6 provide the timeseries analysis

This PVR is accompanied by an annex document (Ref: EUM/21/SAC/PVR-A), which provides the full set of results, when only a selection is provided in the PVR.

The general approach (method and products) of this PVR follows the work carried out in the EUMETSAT SACSO project [AD-3].

1.3 APPLICABLE DOCUMENTS

[AD-1]	OC-SAC Requirement Baseline Document. EUMETSAT deliverable ref. EUM/21/SAC/RB, version 2.1
[AD-2]	OC-SAC Algorithm Theoretical Basis Document. EUMETSAT deliverable ref. EUM/21/SAC/ATBD, version 4.1
[AD-3]	SACSO Product Validation Report. EUMETSAT deliverable ref. EUM/19/SACSO/PVR, version 2.2, available from: https://www.eumetsat.int/SACSO
[AD-4]	Sentinel-3 OLCI L2 report for baseline collection OL_L2M_003. EUMETSAT report ref. EUM/RSP/REP/21/1211386, v2B, 16 April 2021.

2 CONFIGURATION OF THE PROCESSORS

2.1 IPF

In this document, IPF refers to the operational OLCI Level-2 processor of EUMETSAT, as of Processing Baseline 2.73. This corresponds to OLCI Baseline Collection 003.01 (i.e. IPF-OL-2 version 07.01), see [AD-4]. Considering latest collection 003.02 could be considered for future version.

The following IPF flags are applied in this document: CLOUD, CLOUD_AMBIGUOUS, CLOUD_MARGIN, INVALID, COSMETIC, SATURATED, SUSPECT, HISOLZEN, HIGHGLINT, SNOW_ICE, AC_FAIL, WHITECAPS, RWNEG_O2, RWNEG_O3, RWNEG_O4, RWNEG_O5, RWNEG_O6, RWNEG_O7, RWNEG_O8, ADJAC

2.2 OC-SAC

Data produced with the OC-SAC module comes from OLCI Level-1b products, with IPF-OL-1-EO version between 06.07 and 06.12 depending on the scenes. This is theoretically consistent with the IPF Level-2 products processed at EUMETSAT.

Data are generated by the OC-SAC-SACSO prototype, i.e. by the OC-SAC module embedded in the SACSO Level-2 prototype. The algorithm is described in ATBD version 4.0 [AD-2], and notably includes:

- SVC gains in the visible and NIR bands specifically computed for OC-SAC, as shown on Figure 1. This concerns OLCI-A, essentially used in the PVR. Specific gains for OLCI-B remain to be computed. We refer to [AD-2] for more detailed analysis about these SVC gains.
- Rayleigh computed in Spherical Shell geometry.
- BPC with 6 bands, as operationally in Collection 3.
- Two families of aerosol models: standard and strongly absorbing, each one with 9 fine mode fractions, further dependent on 6 relative humidity's (i.e. 108 models in total)
- Aerosol layer height detected with O2 bands, then interpolated among three values in aerosol reflectance computation
- Smile effect correction directly on final marine reflectance

For match-ups and global maps, marine reflectance is fully normalised for BRDF effect within OC-SAC-SACSO (after OC-SAC) with the standard Morel et al. (2002) approach (f/Q LUTs).

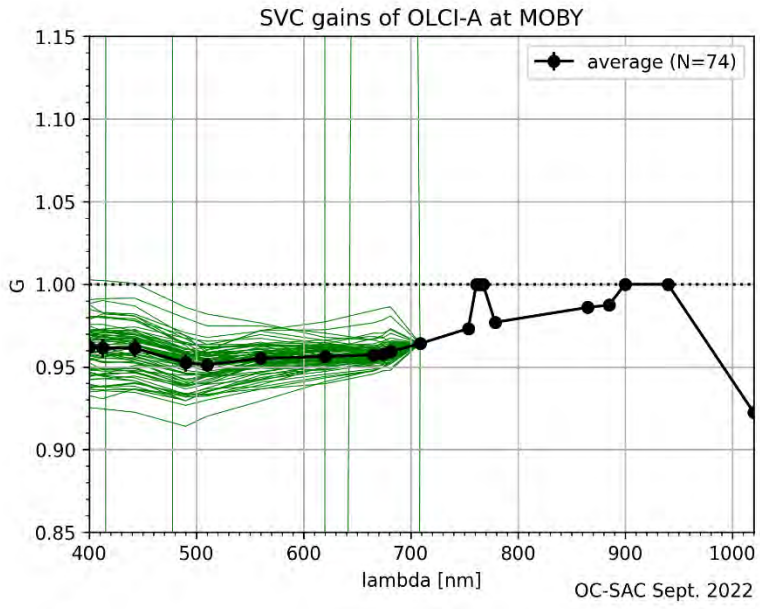

Figure 1: SVC gains used for OC-SAC

The following OC-SAC flags are applied in this document: CLOUD, HIGHGLINT, ACFAIL, SNOW_ICE, WHITECAPS, RWNEG_O2, RWNEG_O3, RWNEG_O4, RWNEG_O5, RWNEG_O6, RWNEG_O7, RWNEG_O8

Note: the CLOUD mask from OC-SAC is currently a simple threshold on the reflectance at 865nm, and is not comparable with the IPF CLOUD mask.

3 VALIDATION WITH IN-SITU DATA

3.1 METHOD AND STATISTICS

A validation is performed using OLCI extractions of AERONET-OC matchups (EUMETSAT Matchup-Database, MDB). The two families of products described in section 2 are validated.

The following statistical variables are used:

- Mean difference: $MD = \frac{1}{n}\sum \rho_{w,OLCI}(\lambda) - \rho_{w,insitu}(\lambda)$ *(accuracy)*
- residual error = $stdev(\rho_{w,OLCI}(\lambda) - \rho_{w,insitu}(\lambda))$ *(precision)*
- Other metrics, as recommended by EUMETSAT:
  - Mean absolute difference: $MAD = \frac{1}{n}\sum |\rho_{w,OLCI}(\lambda) - \rho_{w,insitu}(\lambda)|$
  - Mean Percent Difference: $MPD = \frac{100}{n}\sum \frac{\rho_{w,OLCI}(\lambda) - \rho_{w,insitu}(\lambda)}{\rho_{w,insitu}(\lambda)}$
  - Mean Absolute Percent difference: $MAPD = \frac{100}{n}\sum |\frac{\rho_{w,OLCI}(\lambda) - \rho_{w,insitu}(\lambda)}{\rho_{w,insitu}(\lambda)}|$

The maximum time difference between satellite and in-situ observations is **1 hour**. The validation uses first MOBY for which results are presented independently as a verification, and then several other AERONET-OC sites presented without MOBY. Two sets of validation are considered, following the approach used in Ocean Colour CCI:

- Individual Best Quality (IBQ): the flags are applied per-processor, leading to a different number of validation points for each processor. These results are not presented here because of the incomplete flagging of OC-SAC.
- Common Best Quality (CBQ): the flags are shared, and only the pixels valid for all processors are considered.

Note: the matchup protocol is temporarily different from the recommended OLCI matchup protocol. Notably, the present analysis is done only on the central part of the match-up, not on the average of the macro-pixel. A task of homogenisation of the protocol is planned in the near future.

Flags visualization

A visualization of the considered IPF and OC-SAC flags (see section 2) has been generated for each validation site. This graph can be used as a diagnosis tool to identify the reason for pixels rejection.

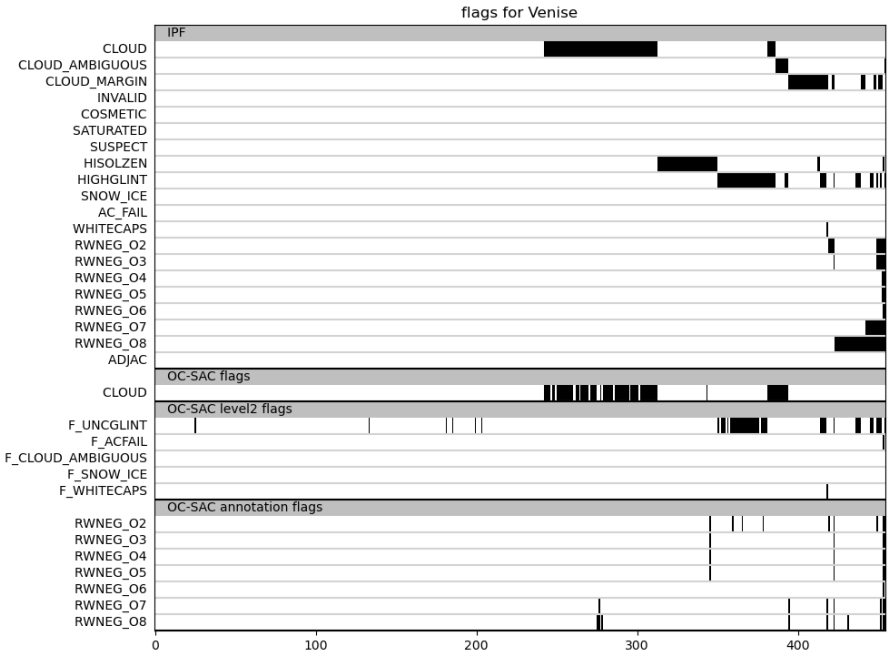

Figure 2: Flags visualization for the CBQ pixels (Venise match-ups). The x axis corresponds to the matchups, for which the flags are displayed in black. Each flag is shown on the y axis. The pixels are sorted by value instead of time, to facilitate the visualization. The full set of such graphs, for all matchup sites, is provided in the annex document.

3.2 RESULTS FOR MOBY

3.2.1 IBQ PLOTS

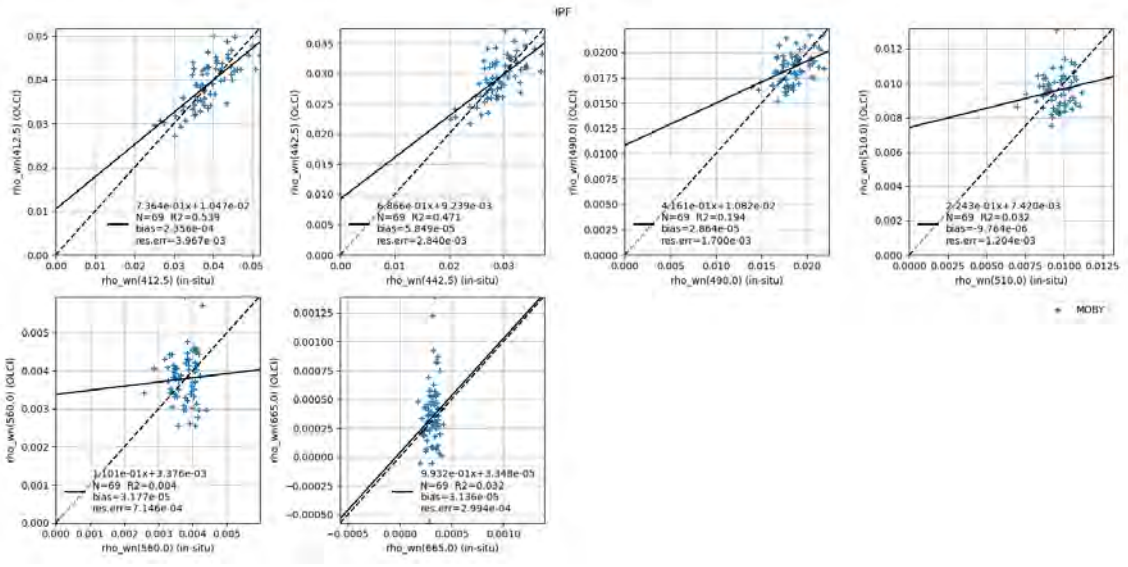

Figure 3: IPF validation results

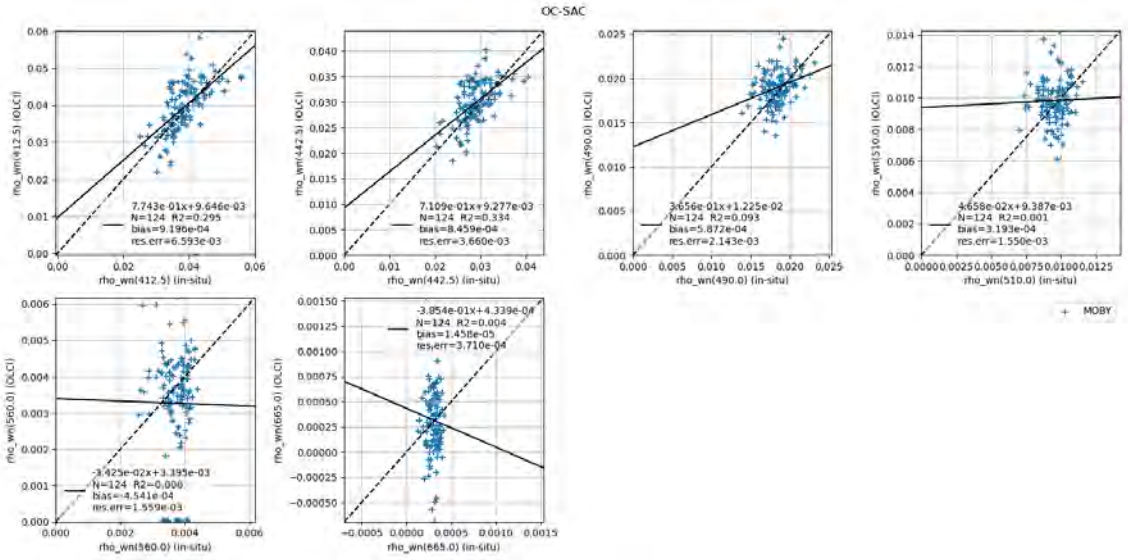

Figure 4: OC-SAC validation results

3.2.2 IBQ STATISTICS

3.2.2.1 IPF

Wav.	N	R2	bias	reserr	MD	MAD	MAPD	MPD
412.5	69	0.538969	0.000236	0.003967	0.000236	0.003317	8.612544	1.123228
442.5	69	0.471170	0.000058	0.002840	0.000058	0.002295	7.865447	0.664845
490.0	69	0.194182	0.000029	0.001700	0.000029	0.001437	7.884535	0.638916
510.0	69	0.031842	-0.000010	0.001204	-0.000010	0.001006	10.605028	0.513746
560.0	69	0.003519	0.000032	0.000715	0.000032	0.000564	15.112736	1.699969
665.0	69	0.032473	0.000031	0.000299	0.000031	0.000212	68.597326	10.181290

3.2.2.2 OC-SAC

Wav.	N	R2	bias	reserr	MD	MAD	MAPD	MPD
412.5	124	0.294939	0.000920	0.006593	0.000920	0.004576	12.009563	2.805373
442.5	124	0.334465	0.000846	0.003660	0.000846	0.002943	10.322969	3.320025
490.0	124	0.093221	0.000587	0.002143	0.000587	0.001742	9.797096	3.742879
510.0	124	0.000923	0.000319	0.001550	0.000319	0.001226	13.345097	4.230386
560.0	124	0.000073	-0.000454	0.001559	-0.000454	0.001121	30.792281	-11.022183
665.0	124	0.004346	0.000015	0.000371	0.000015	0.000276	98.117465	13.633019

3.2.3 IBQ SUMMARY STATISTICS

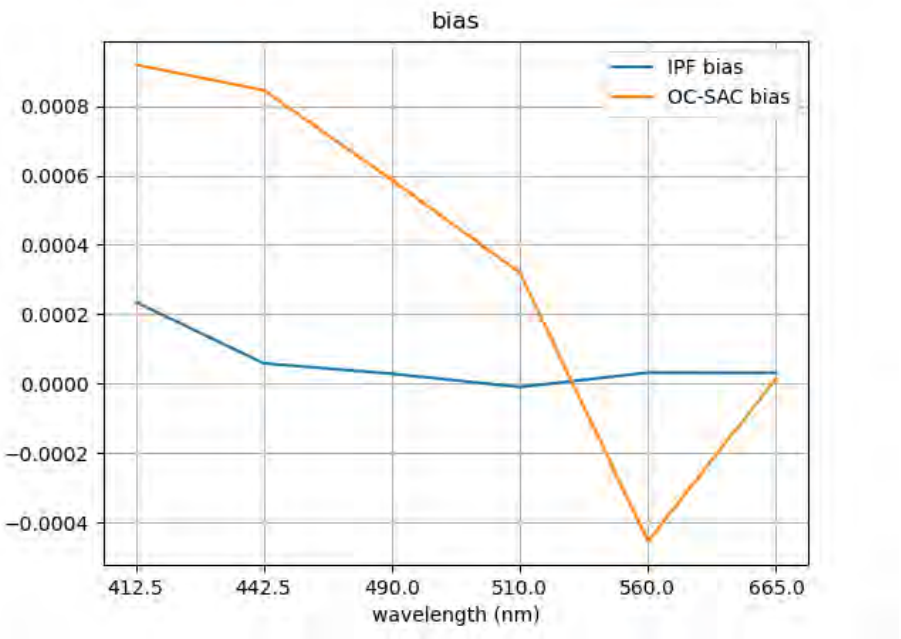

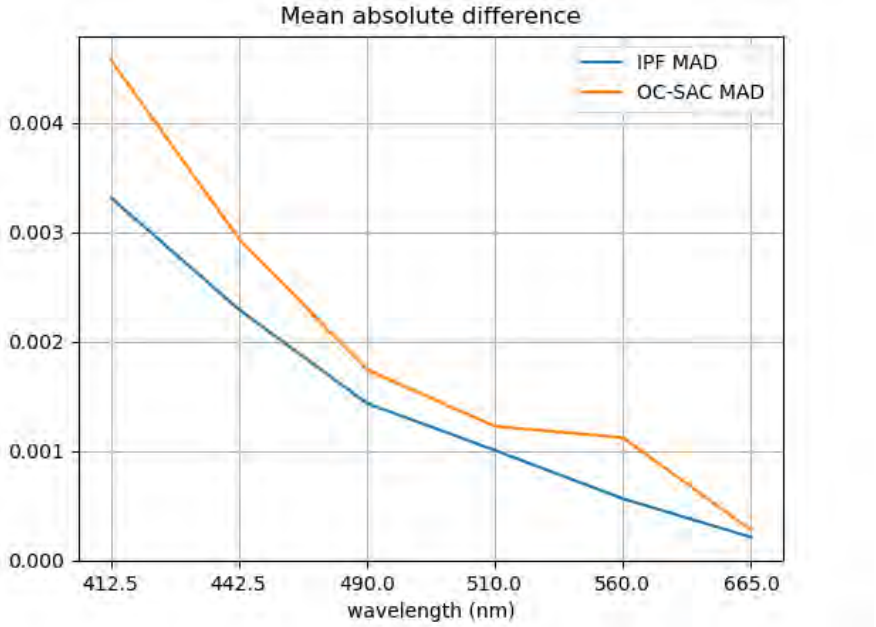
Mean absolute difference
IPF MAD
OC-SAC MAD
0.004
0.003
0.002
0.001
0.000
412.5
442.5
490.0
510.0
560.0
665.0
wavelength (nm)

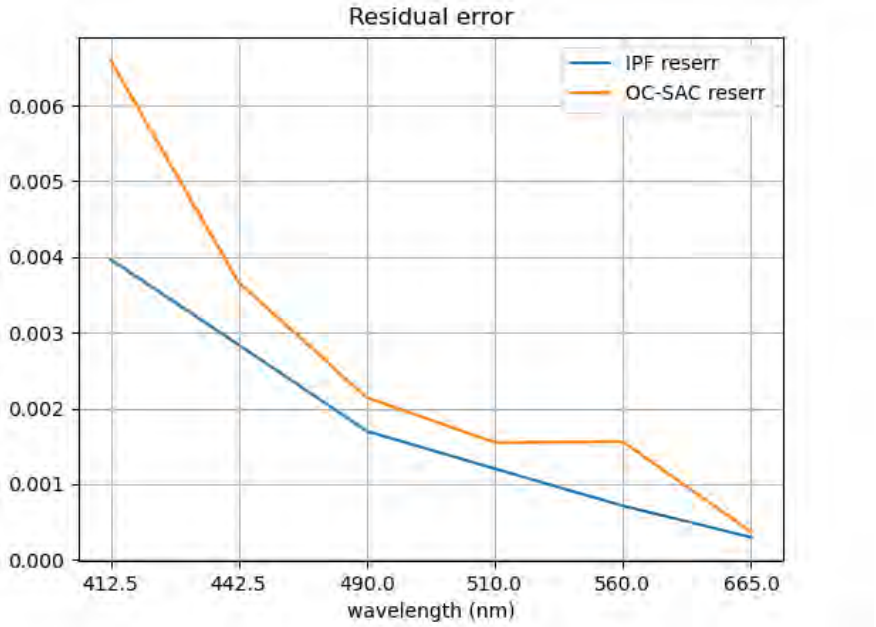
Residual error
IPF reserr
OC-SAC reserr
0.006
0.005
0.004
0.003
0.002
0.001
0.000
412.5
442.5
490.0
510.0
560.0
665.0
wavelength (nm)

3.2.4 CBQ PLOTS

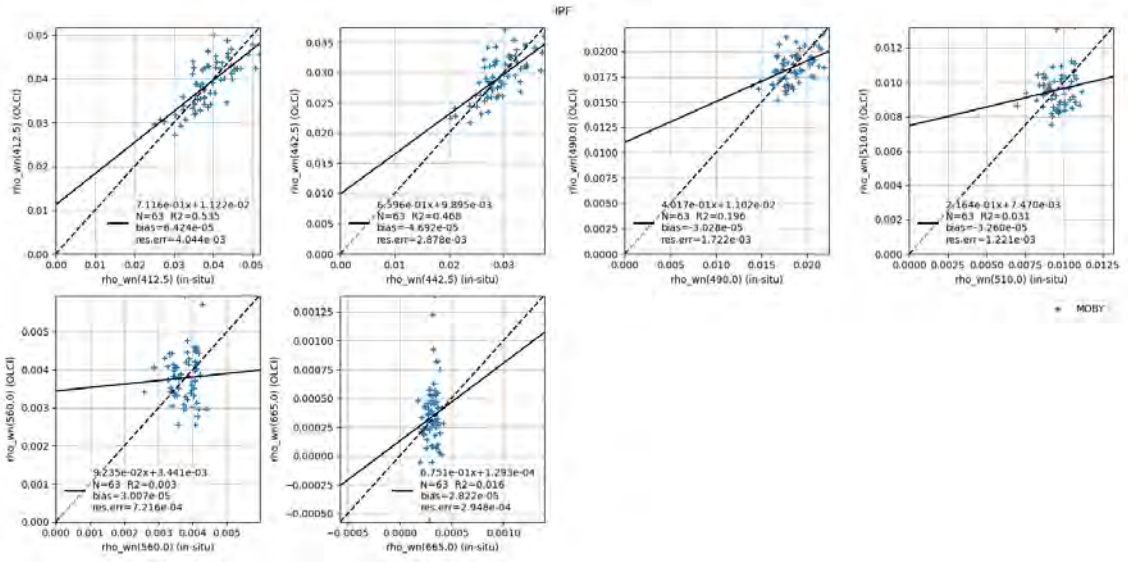

Figure 5: IPF validation results

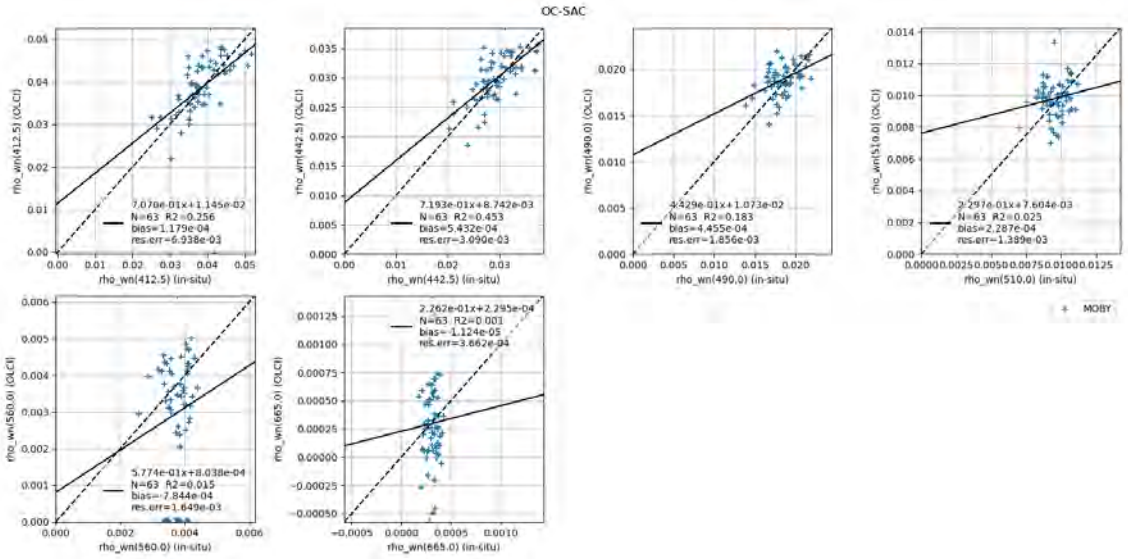

Figure 6: OC-SAC validation results

3.2.5 CBQ STATISTICS

3.2.5.1 IPF

Wav.	N	R2	bias	reserr	MD	MAD	MAPD	MPD
412.5	63	0.535248	0.000064	0.004044	0.000064	0.003365	8.762063	0.759812
442.5	63	0.468177	-0.000047	0.002878	-0.000047	0.002313	7.948001	0.368871
490.0	63	0.196282	-0.000030	0.001722	-0.000030	0.001456	7.996977	0.363237
510.0	63	0.031396	-0.000033	0.001221	-0.000033	0.001015	10.708705	0.321293
560.0	63	0.002604	0.000030	0.000722	0.000030	0.000571	15.341669	1.718905
665.0	63	0.015936	0.000028	0.000295	0.000028	0.000204	65.384412	10.240664

3.2.5.2 OC-SAC

Wav.	N	R2	bias	reserr	MD	MAD	MAPD	MPD
412.5	63	0.255920	0.000118	0.006938	0.000118	0.004203	10.995699	0.927247
442.5	63	0.453099	0.000543	0.003090	0.000543	0.002522	8.865260	2.323085
490.0	63	0.183407	0.000446	0.001856	0.000446	0.001553	8.696095	2.926412
510.0	63	0.024881	0.000229	0.001389	0.000229	0.001113	11.916801	3.054024
560.0	63	0.015488	-0.000784	0.001649	-0.000784	0.001298	35.106018	-20.529601
665.0	63	0.001188	-0.000011	0.000366	-0.000011	0.000284	93.671864	-1.441996

3.2.6 CBQ SUMMARY STATISTICS

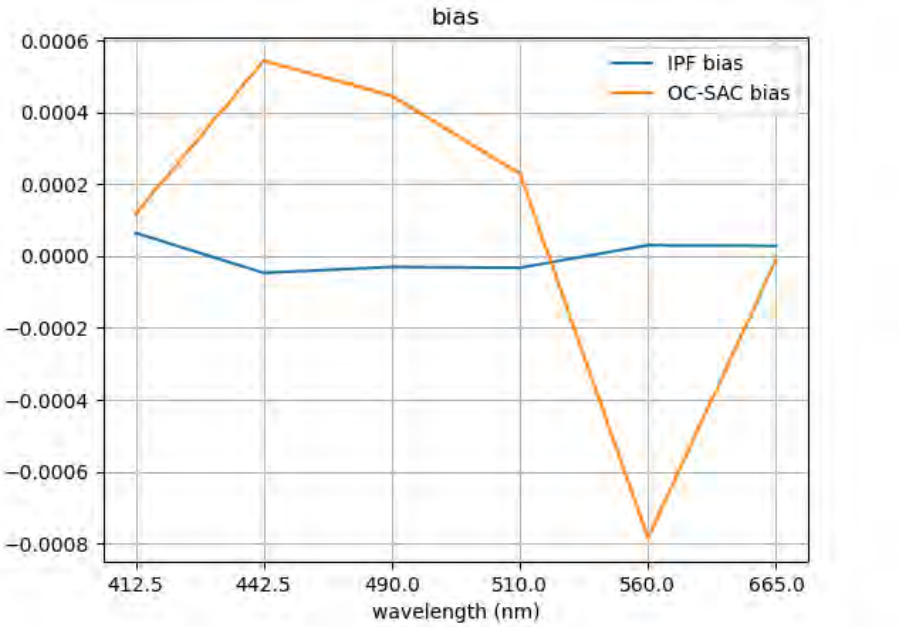

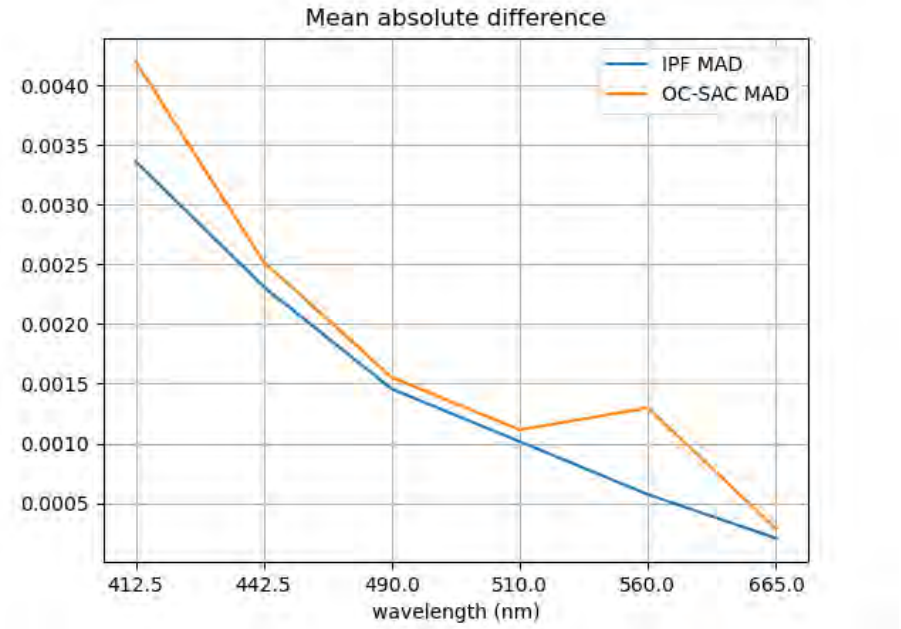

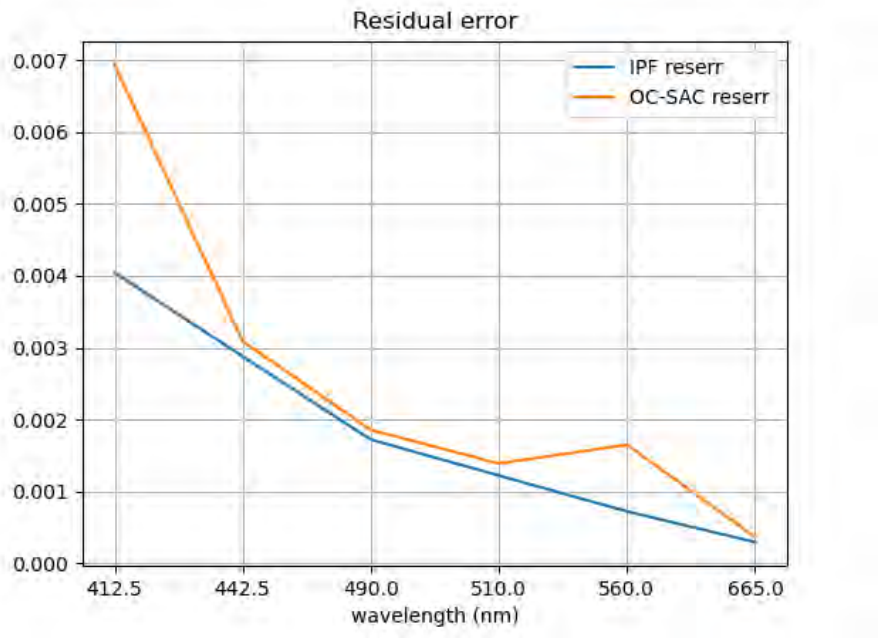
Residual error
IPF reserr
OC-SAC reserr
0.007
0.006
0.005
0.004
0.003
0.002
0.001
0.000
412.5
442.5
490.0
510.0
560.0
665.0
wavelength (nm)

3.3 RESULTS FOR AERONET-OC

3.3.1 IBQ PLOTS

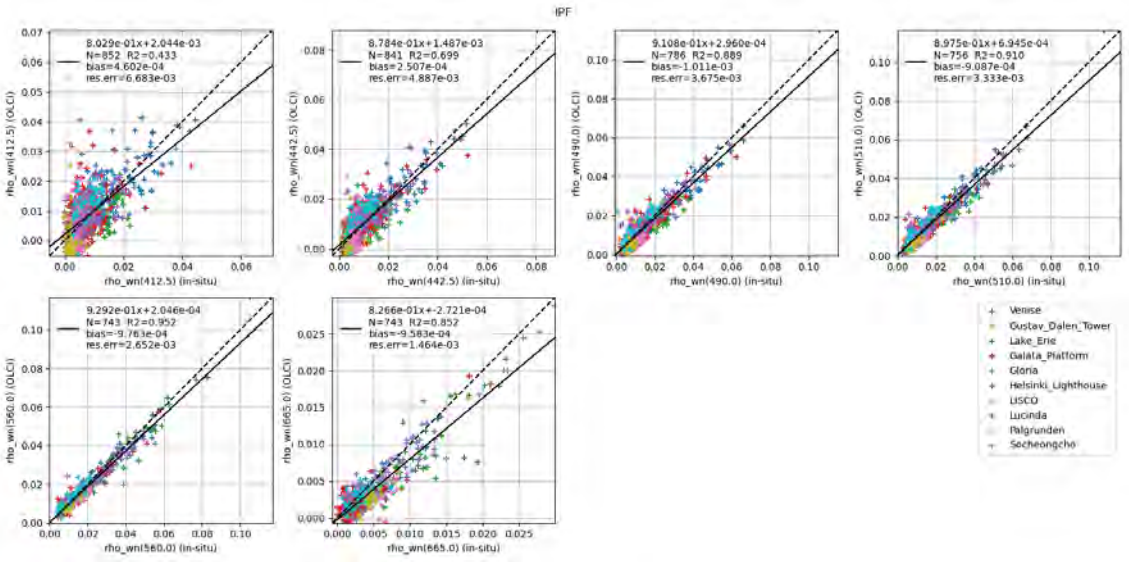

Figure 7: IPF validation results

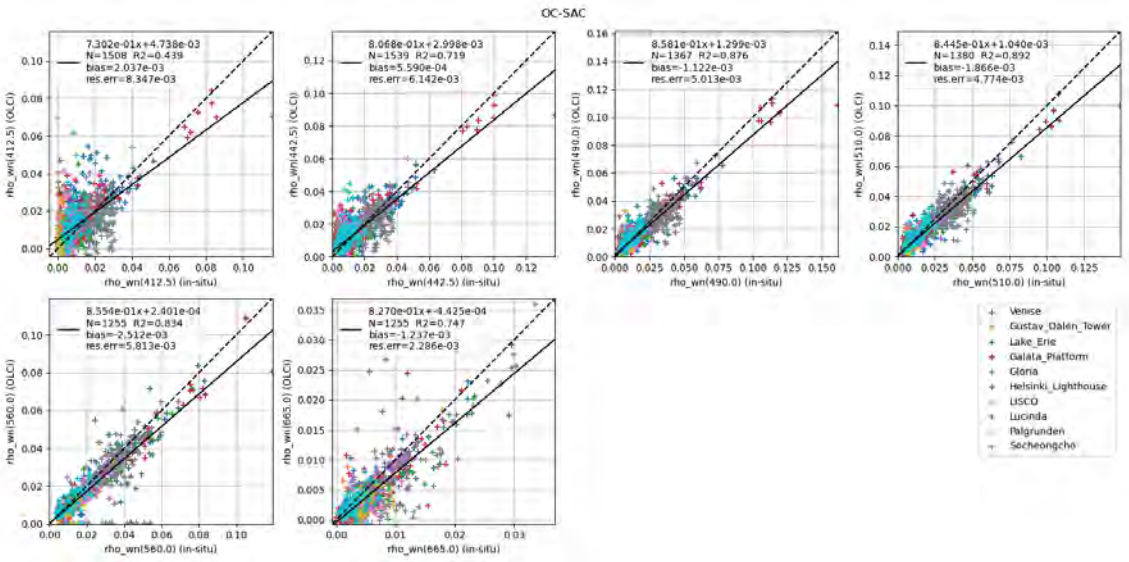

Figure 8: OC-SAC validation results

3.3.2 IBQ STATISTICS

3.3.2.1 IPF

Wav.	N	R2	bias	reserr	MD	MAD	MAPD	MPD
412.5	852	0.433485	0.000460	0.006683	0.000460	0.004961	266.772632	80.673974
442.5	841	0.698669	0.000251	0.004887	0.000251	0.003775	58.746572	10.025675
490.0	786	0.888897	-0.001011	0.003675	-0.001011	0.002900	39.706628	6.493657
510.0	756	0.910302	-0.000909	0.003333	-0.000909	0.002589	21.059129	-3.286828
560.0	743	0.952408	-0.000976	0.002652	-0.000976	0.002012	14.344562	-4.301189
665.0	743	0.852246	-0.000958	0.001464	-0.000958	0.001280	47.674730	-16.477625

3.3.2.2 OC-SAC

Wav.	N	R2	bias	reserr	MD	MAD	MAPD	MPD
412.5	1508	0.438920	0.002037	0.008347	0.002037	0.005738	281.961513	98.984396
442.5	1539	0.718698	0.000559	0.006142	0.000559	0.004165	54.187995	24.063739
490.0	1367	0.876411	-0.001122	0.005013	-0.001122	0.003323	26.712254	-1.565738
510.0	1380	0.891984	-0.001866	0.004774	-0.001866	0.003416	21.780753	-7.108846
560.0	1255	0.834471	-0.002512	0.005813	-0.002512	0.003606	20.368747	-12.280441
665.0	1255	0.746992	-0.001237	0.002286	-0.001237	0.001732	49.225685	-28.047600

3.3.3 IBQ SUMMARY STATISTICS

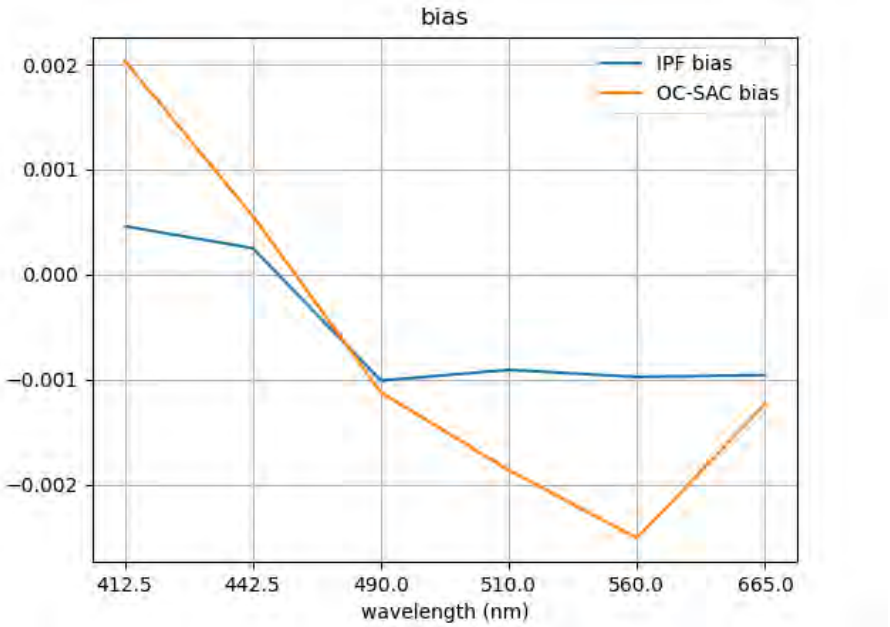

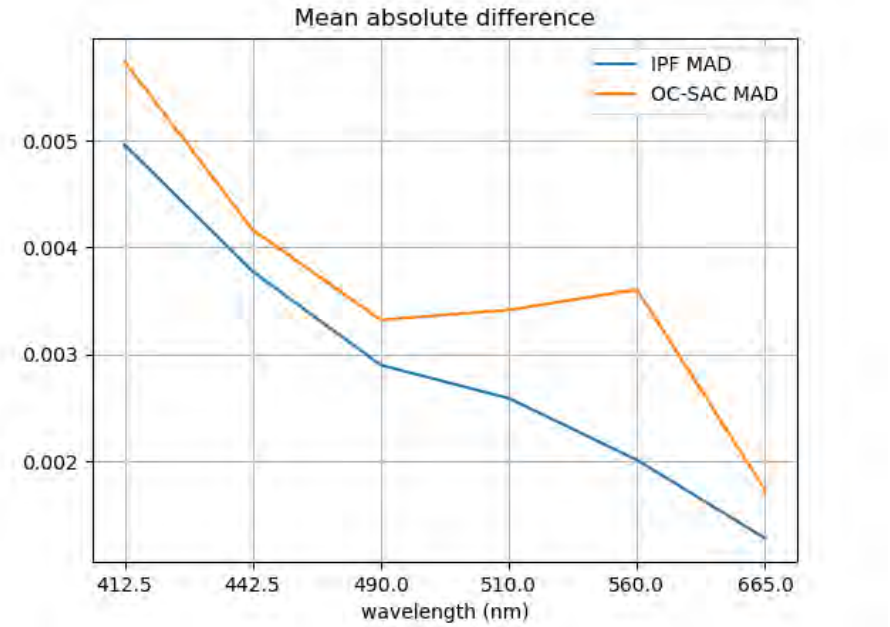

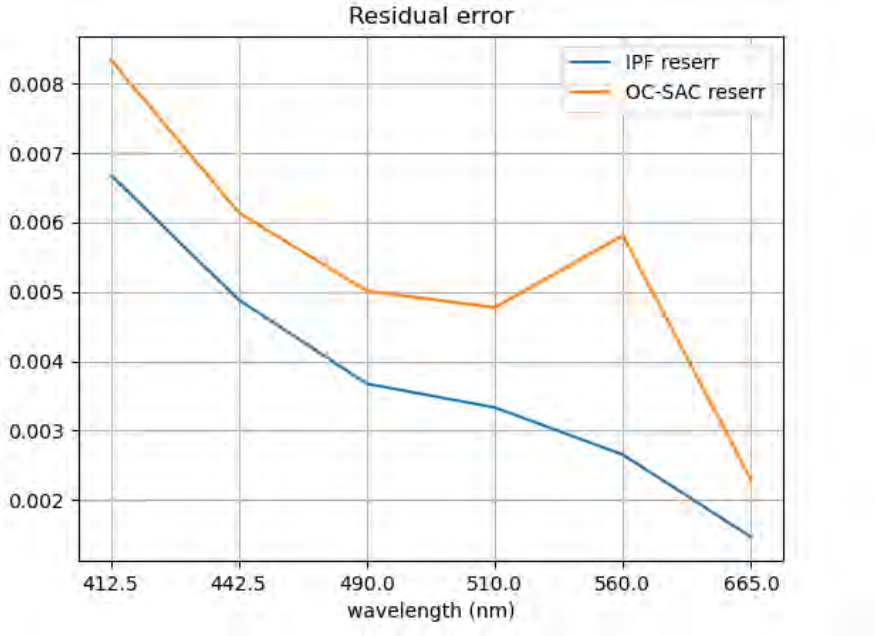
Residual error
IPF reserr
OC-SAC reserr
0.008
0.007
0.006
0.005
0.004
0.003
0.002
412.5
442.5
490.0
510.0
560.0
665.0
wavelength (nm)

3.3.4 CBQ PLOTS

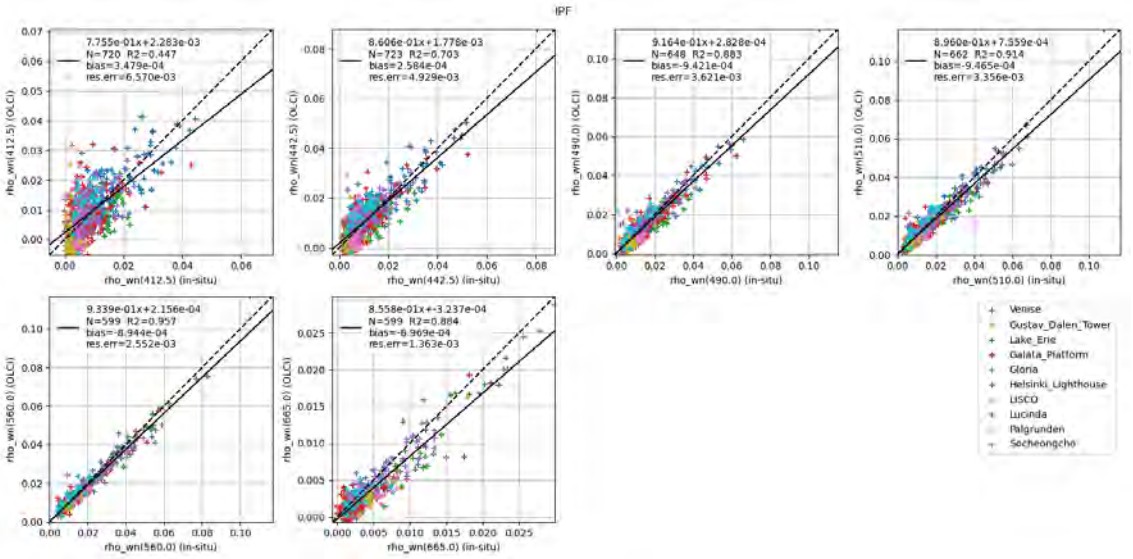

Figure 9: IPF validation results

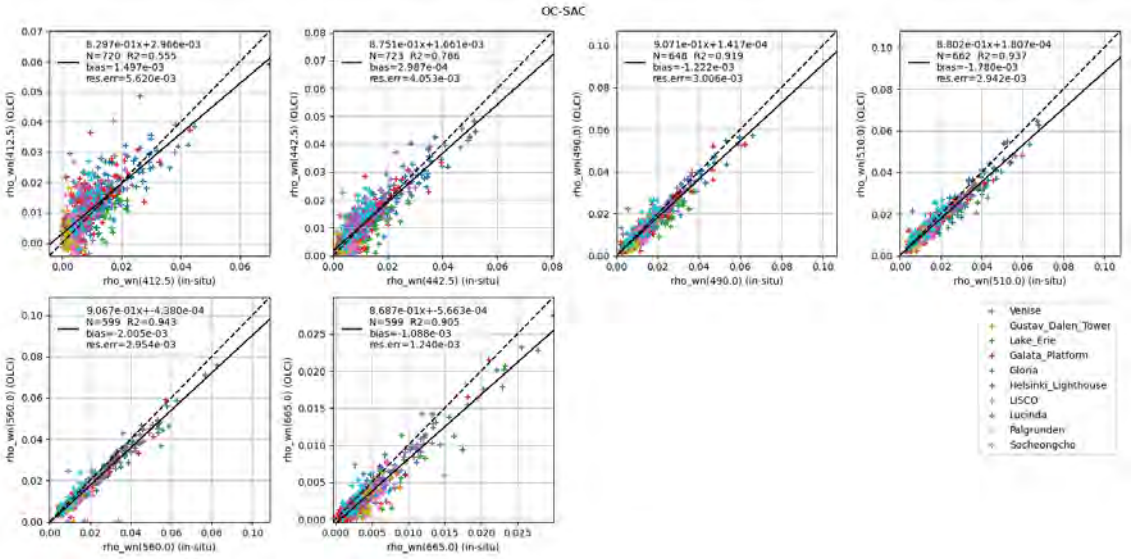

Figure 10: OC-SAC validation results

3.3.5 CBQ STATISTICS

3.3.5.1 IPF

Wav.	N	R2	bias	reserr	MD	MAD	MAPD	MPD
412.5	720	0.447153	0.000348	0.006570	0.000348	0.004914	231.251355	68.548748
442.5	723	0.703344	0.000258	0.004929	0.000258	0.003807	54.211293	12.873496
490.0	648	0.883148	-0.000942	0.003621	-0.000942	0.002831	41.346450	10.394093
510.0	662	0.914368	-0.000947	0.003356	-0.000947	0.002611	20.099052	-2.879672
560.0	599	0.957208	-0.000894	0.002552	-0.000894	0.001938	13.779929	-3.713767
665.0	599	0.883826	-0.000897	0.001363	-0.000897	0.001227	48.639231	-14.529330

3.3.5.2 OC-SAC

Wav.	N	R2	bias	reserr	MD	MAD	MAPD	MPD
412.5	720	0.554991	0.001497	0.005620	0.001497	0.004249	172.987676	89.481139
442.5	723	0.785784	0.000299	0.004053	0.000299	0.002999	40.299660	12.153789
490.0	648	0.918535	-0.001222	0.003006	-0.001222	0.002363	20.892635	-6.335838
510.0	662	0.937365	-0.001780	0.002942	-0.001780	0.002516	17.677027	-9.736606
560.0	599	0.943360	-0.002005	0.002954	-0.002005	0.002381	15.634611	-12.162466
665.0	599	0.904620	-0.001088	0.001240	-0.001088	0.001242	43.753791	-30.064282

3.3.6 CBQ SUMMARY STATISTICS

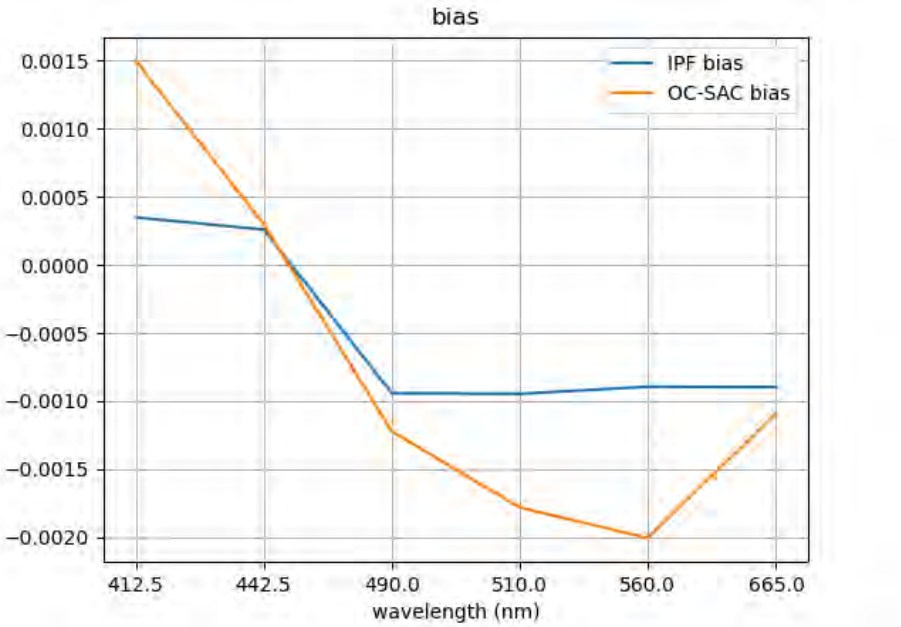

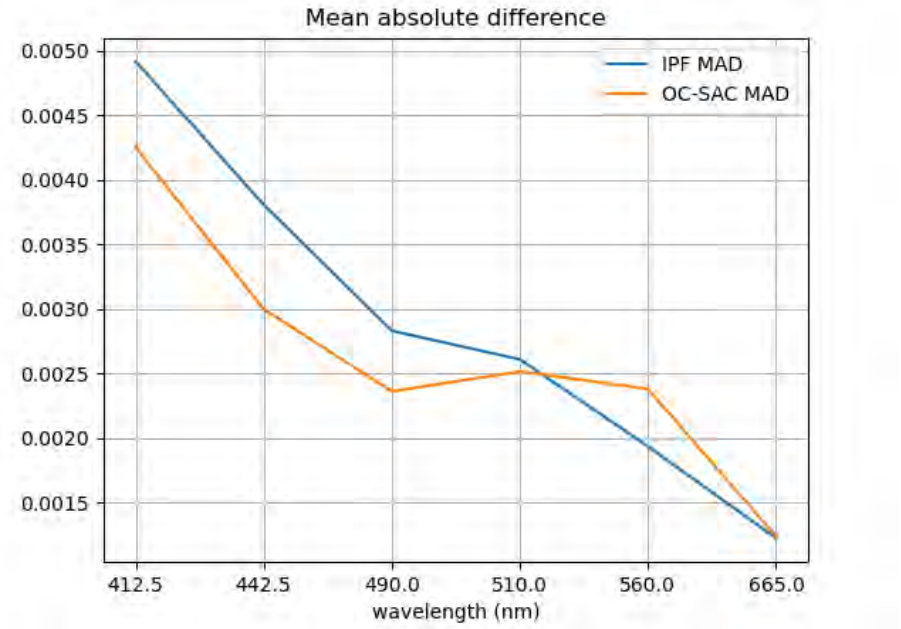

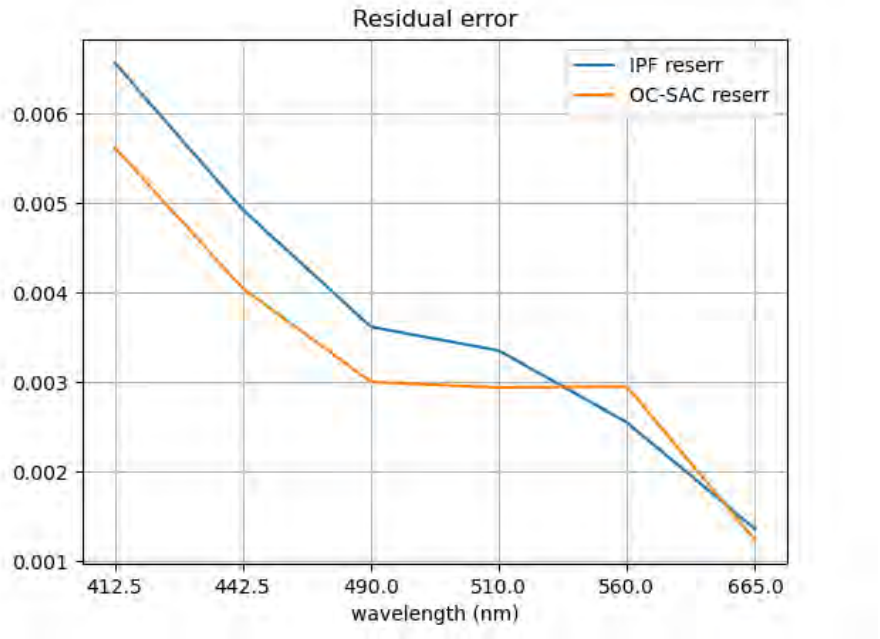
Residual error
IPF reserr
OC-SAC reserr
0.006
0.005
0.004
0.003
0.002
0.001
412.5
442.5
490.0
510.0
560.0
665.0
wavelength (nm)

4 SAMPLE SCENES VISUALIZATION

4.1 METHOD

In this section, the scenes from the diagnostic dataset are shown as RGB composites. This method was developed in the SACSO project [AD-3]. A subset of all results is shown in this document; the full set of OLCI images is provided in the Annex.

For each OLCI image, a RGB visualization is provided for the TOA reflectance, and for the water reflectance (rho_w) estimated by each processor.

The images are RGB composites using the bands R=665, G=560 and B=443.

- The full top of atmosphere reflectance ρ_{toa}
- The water reflectance ρ_w

The colour scaling v is performed consistently for all images, using a log scale:

$$v = \frac{\ln(1 + 100 \cdot \rho)}{\ln(1 + 100 \cdot \rho_{max})} \quad (1)$$

Where ρ is the input reflectance at any of the three band, and ρ_{max} is equal to 1 for ρ_{toa}, and 0.1 for ρ_w. This log scaling is applied to enhance the contrast towards low values of ρ. The final colour is given by the triplet of values of $v \in [0, 1]$ at the R, G and B bands.

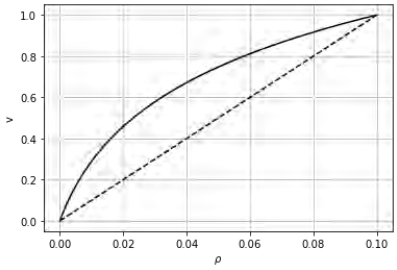

Figure 11: plot of equation (1) for $\rho_{max} = 0.1$ (solid line)

Pixels where $\rho > \rho_{max}$ at any of the three R, G or B bands, are shown in **white**. Pixels where $\rho < 0$ at any of the three R, G or B bands, are shown in **black**. Invalid values (NaN) are shown in **grey**.

This visualization intends to show the **natural colour of the water**: for ρ_w, the RGB will appear in general blue over the clear waters, and becomes green and possibly yellow over more complex waters. Further, masks are alternatively displayed on the images.

This qualitative visualization is complemented by a more quantitative evaluation in other sections.

Flags are alternatively displayed in red. See section 2 for the description of the included flags.

In addition to the RGB composites for rho_toa and rho_w, other useful parameters are displayed: Ångström coefficient, aerosol model index and optical thickness at 865nm.

4.2 RESULTS: SELECTION OF SCENES

4.2.1 1-3_NORTH_BALTIC_SEA

Product name is:
S3A_OL_1_EFR____20180507T092500_20180507T092800_20180508T134443_0179_031_036_1980_LN1_O_NT_002.SEN3.oc-sac.nc

Figure 12: RGB colour composite of rho_toa for Case 1-3_North_Baltic_Sea

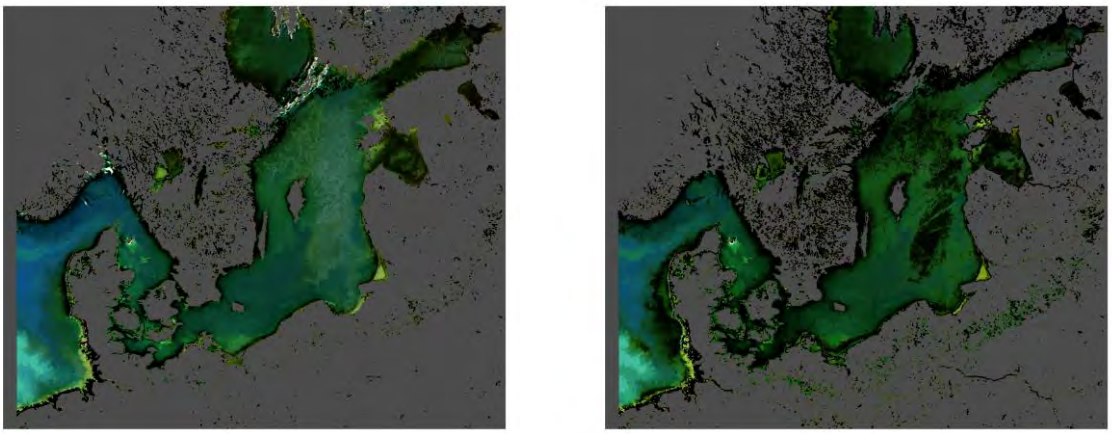

Figure 13: RGB colour composite of rho_w from OC-SAC (left) and IPF (right) for Case 1-3_North_Baltic_Sea

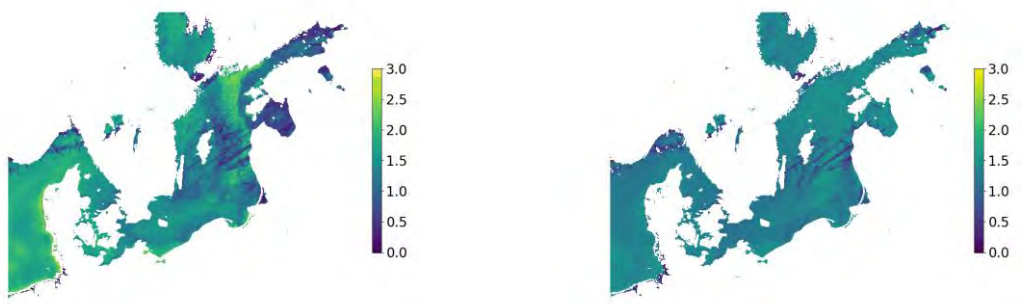

Figure 14: Ångström coefficient from OC-SAC (left) and IPF (right) for Case 1-3_North_Baltic_Sea

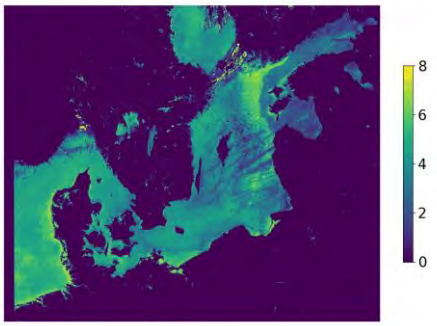

Figure 15: Aerosol model index from OC-SAC for Case 1-3_North_Baltic_Sea

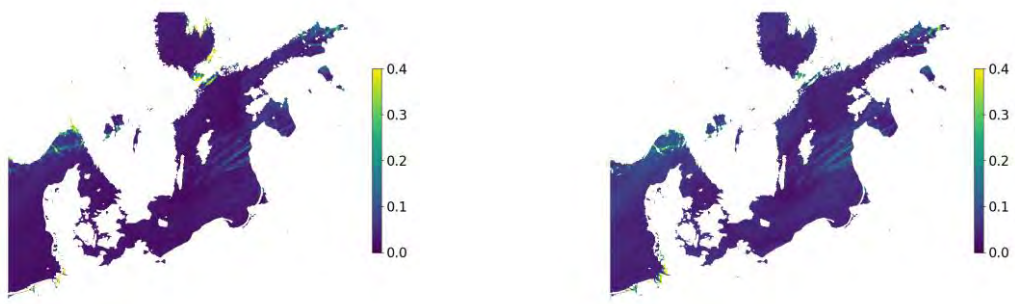

Figure 16: Aerosol optical thickness from OC-SAC (left) and IPF (right) for Case 1-3_North_Baltic_Sea

4.2.2 1-6_MACKENZIE

Product name is:
S3A_OL_1_EFR____20170620T195021_20170620T195321_20180503T164933_0179_019_085_1800_LR2_R_NT_002.SEN3.oc-sac.nc

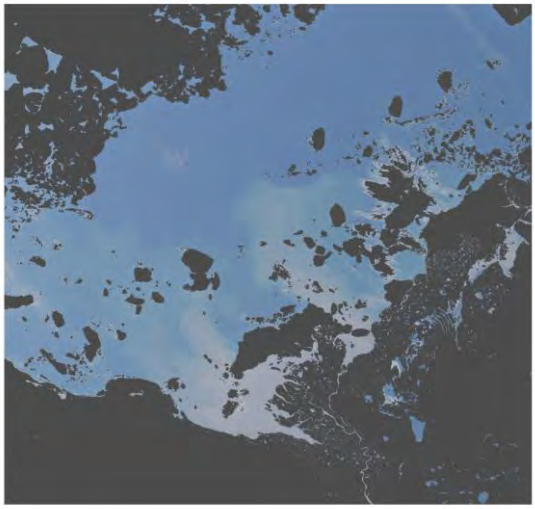

Figure 17: RGB colour composite of rho_toa for Case 1-6_Mackenzie

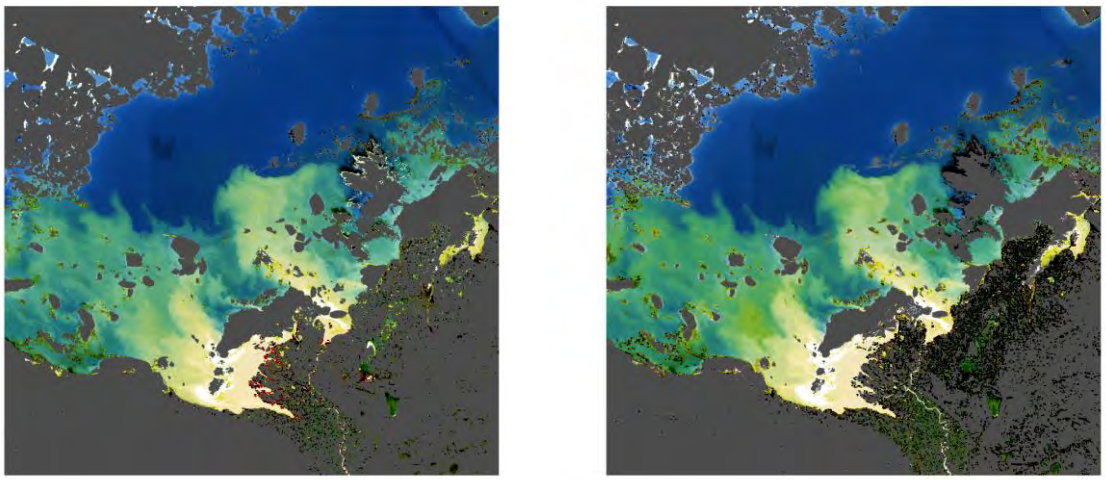

Figure 18: RGB colour composite of rho_w from OC-SAC (left) and IPF (right) for Case 1-6_Mackenzie

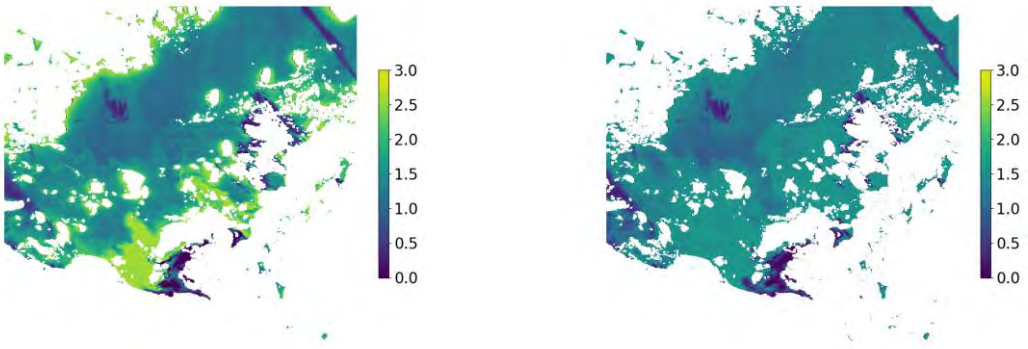

Figure 19: Ångström coefficient from OC-SAC (left) and IPF (right) for Case 1-6_Mackenzie

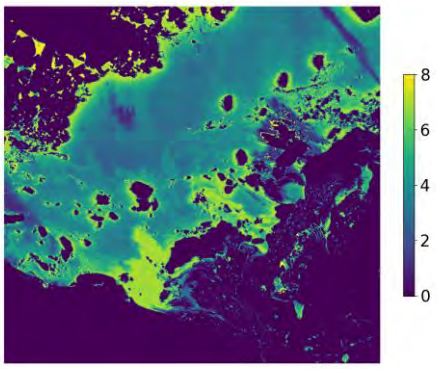

Figure 20: Aerosol model index from OC-SAC for Case 1-6_Mackenzie

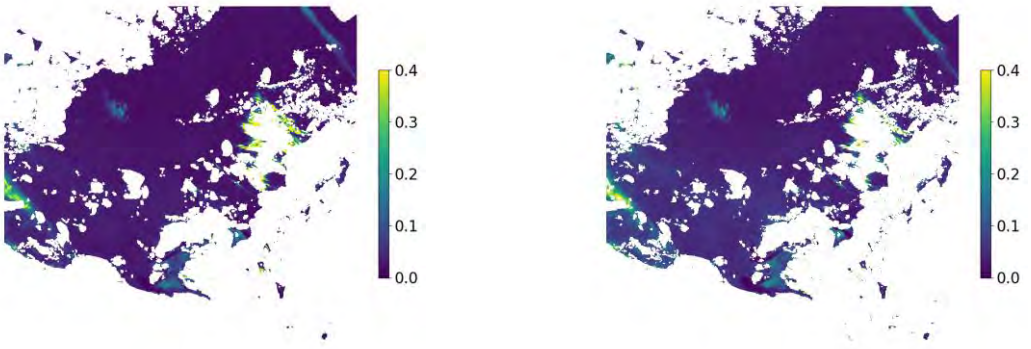

Figure 21: Aerosol optical thickness from OC-SAC (left) and IPF (right) for Case 1-6_Mackenzie

4.2.3 1-8_RIO_DE_LA_PLATA

Product name is:
S3A_OL_1_EFR____20170114T130626_20170114T130826_20171010T225617_0119_013_152_____MR1_R_NT_002.SEN3.oc-sac.nc

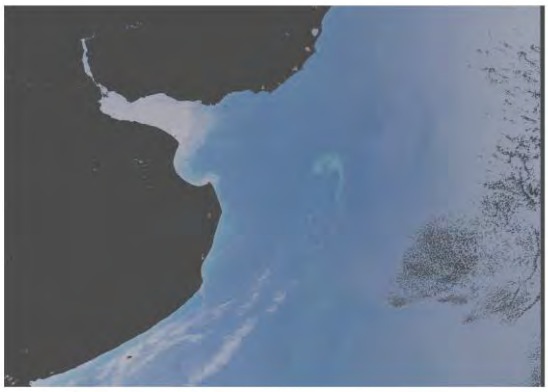

Figure 22: RGB colour composite of rho_toa for Case 1-8_Rio_de_la_Plata

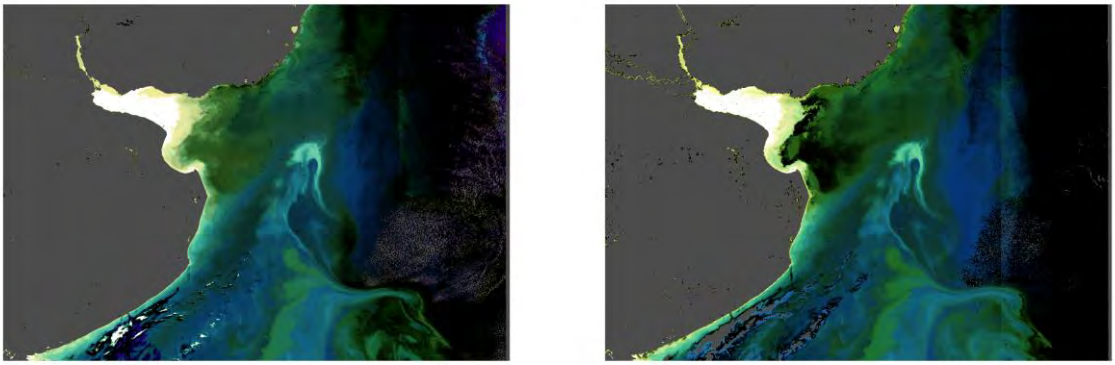

Figure 23: RGB colour composite of rho_w from OC-SAC (left) and IPF (right) for Case 1-8_Rio_de_la_Plata

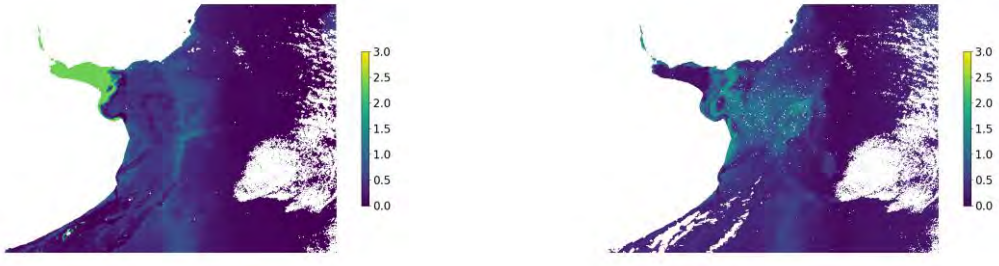

Figure 24: Ångström coefficient from OC-SAC (left) and IPF (right) for Case 1-8_Rio_de_la_Plata

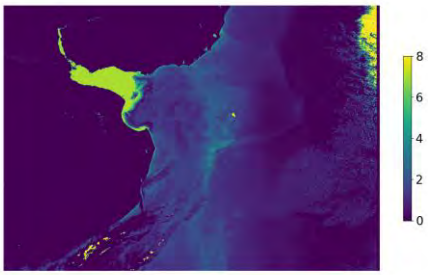

Figure 25: Aerosol model index from OC-SAC for Case 1-8_Rio_de_la_Plata

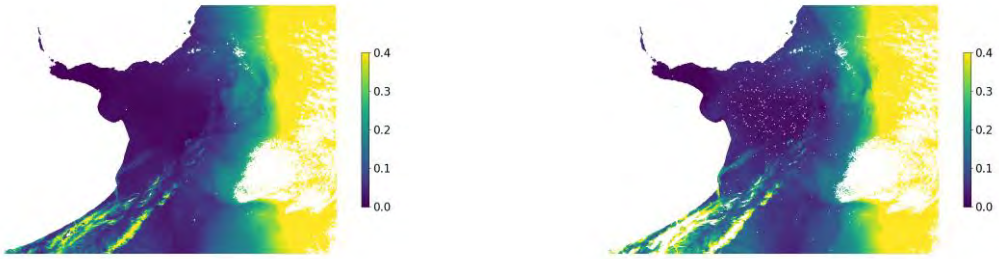

Figure 26: Aerosol optical thickness from OC-SAC (left) and IPF (right) for Case 1-8_Rio_de_la_Plata

4.2.4 1-13_BLACK_SEA

Product name is:
S3A_OL_1_EFR____20170913T080543_20170913T080843_20180713T024026_0179_022_135_2160_LR2_R_NT_002.SEN3.oc-sac.nc

Figure 27: RGB colour composite of rho_toa for Case 1-13_Black_Sea

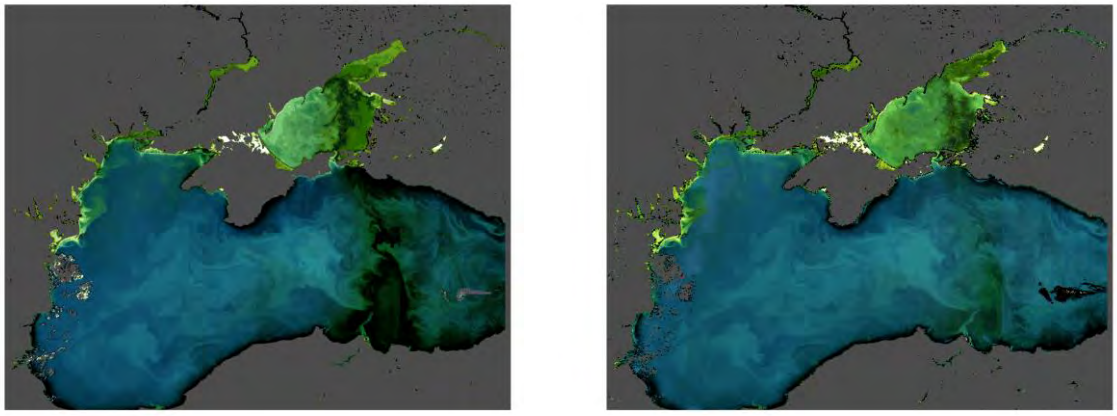

Figure 28: RGB colour composite of rho_w from OC-SAC (left) and IPF (right) for Case 1-13_Black_Sea

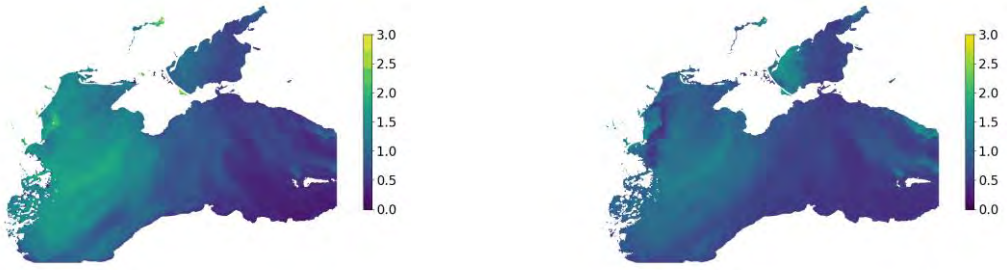

Figure 29: Ångström coefficient from OC-SAC (left) and IPF (right) for Case 1-13_Black_Sea

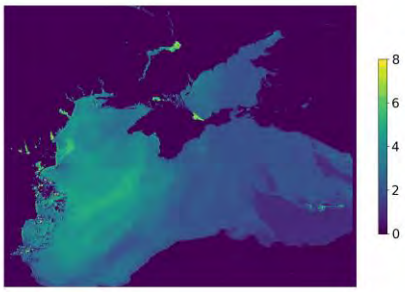

Figure 30: Aerosol model index from OC-SAC for Case 1-13_Black_Sea

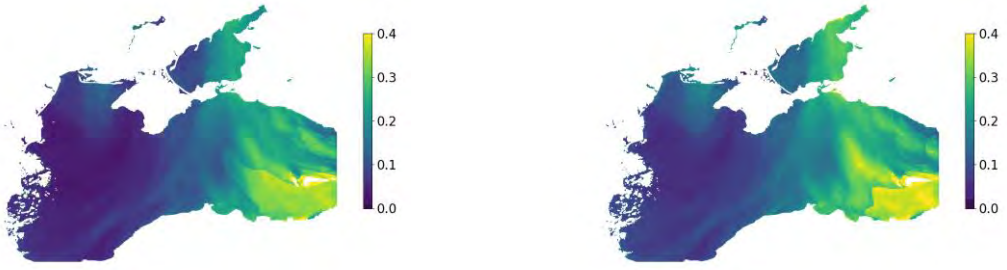

Figure 31: Aerosol optical thickness from OC-SAC (left) and IPF (right) for Case 1-13_Black_Sea

4.2.5 2-1_SAHARA

Product name is:
S3A_OL_1_EFR____20180530T112144_20180530T112444_20180531T150537_0179_031_365_2700_LN1_O_NT_002.SEN3.oc-sac.nc

Figure 32: RGB colour composite of rho_toa for Case 2-1_Sahara

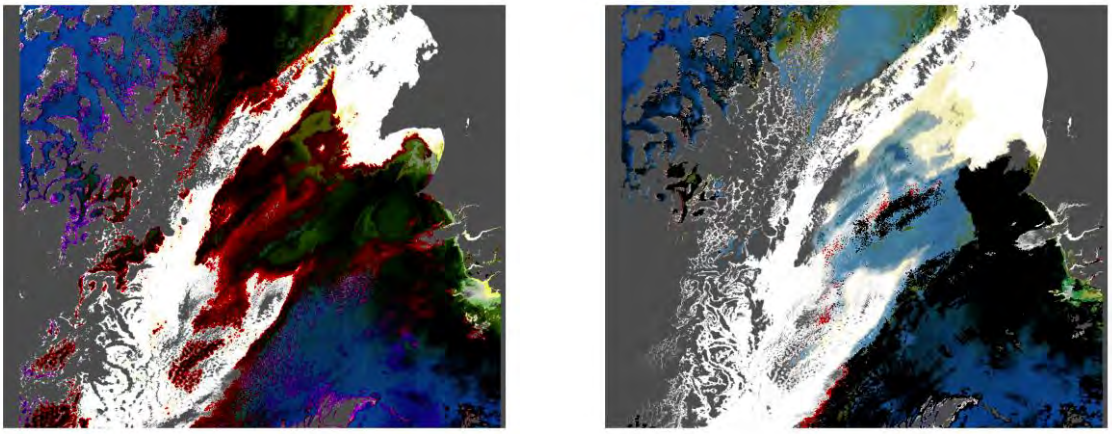

Figure 33: RGB colour composite of rho_w from OC-SAC (left) and IPF (right) for Case 2-1_Sahara

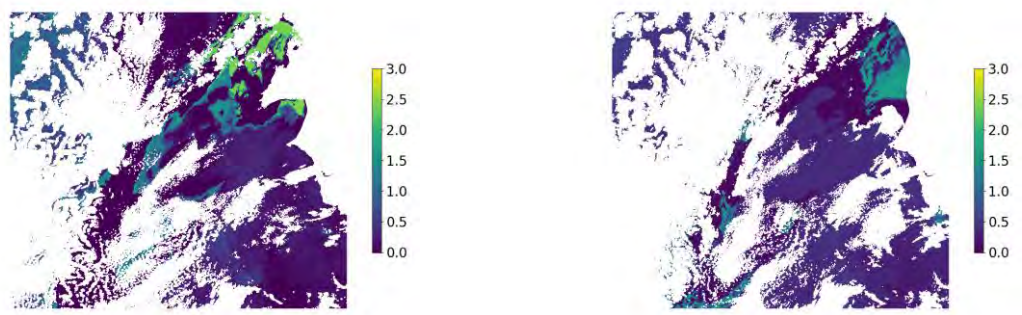

Figure 34: Ångström coefficient from OC-SAC (left) and IPF (right) for Case 2-1_Sahara

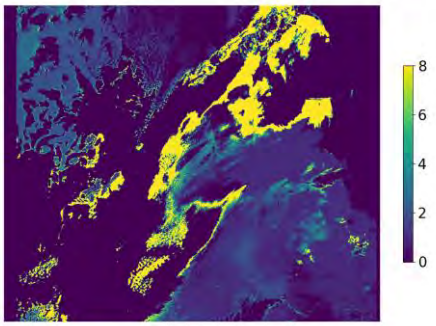

Figure 35: Aerosol model index from OC-SAC for Case 2-1_Sahara

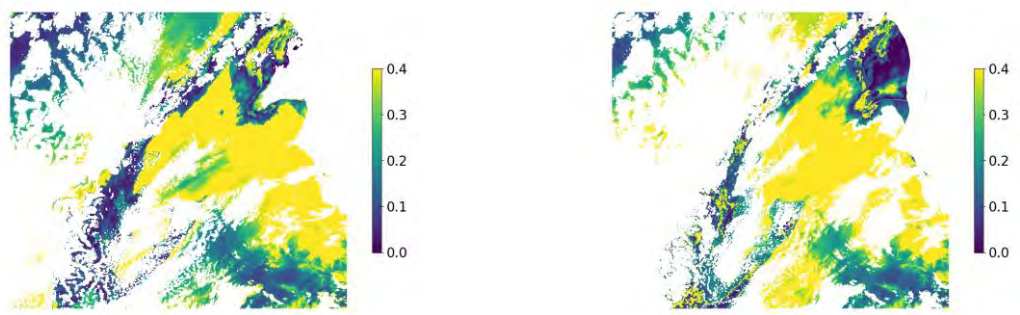

Figure 36: Aerosol optical thickness from OC-SAC (left) and IPF (right) for Case 2-1_Sahara

5 GLOBAL MAPS

5.1 METHOD

Global composites (L3bins) of OC-SAC and IPF are generated over periods of 4 days, for the months of March, June, September and December of 2019. The results are shown for March 2019 in the following section, and for other months in the annex document. Note that there were some missing orbits for OC-SAC.

5.2 RESULTS: 01-04/03/2019

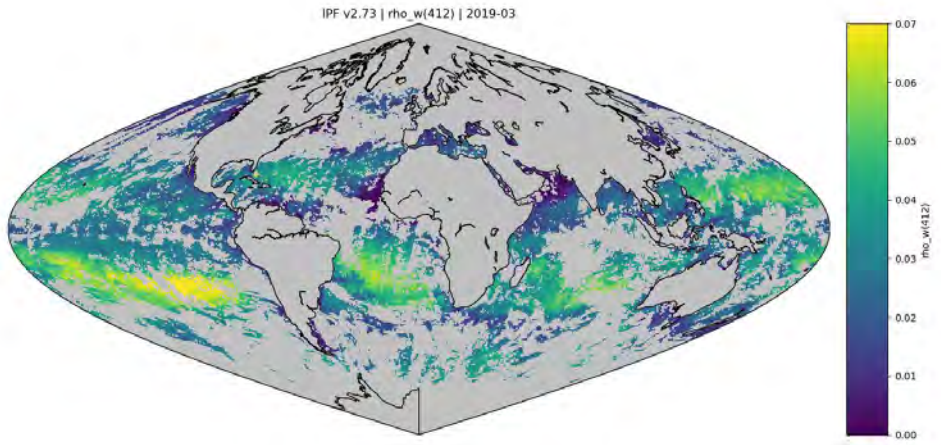

Figure 37: IPF v2.73 | rho_w(412) | 2019-03

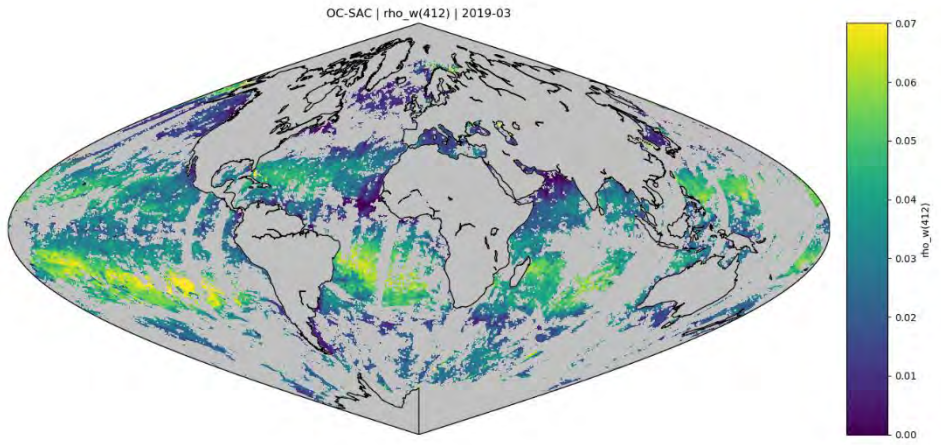

Figure 38: OC-SAC | rho_w(412) | 2019-03

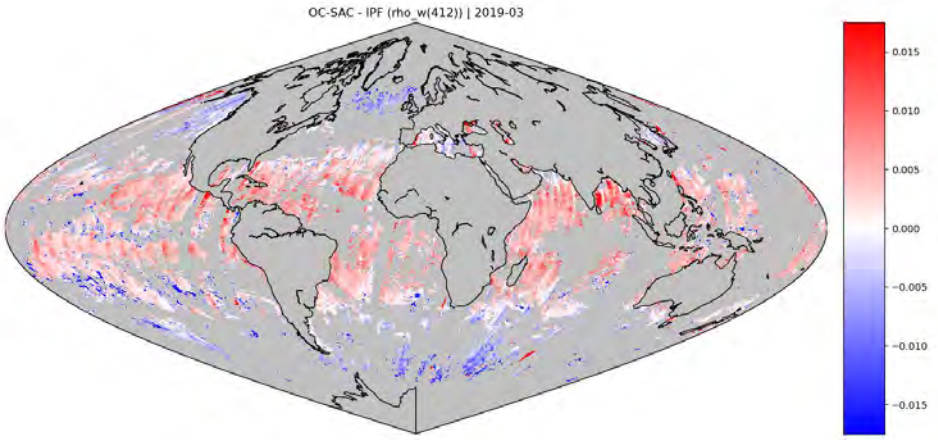

Figure 39: OC-SAC - IPF (rho_w(412)) | 2019-03

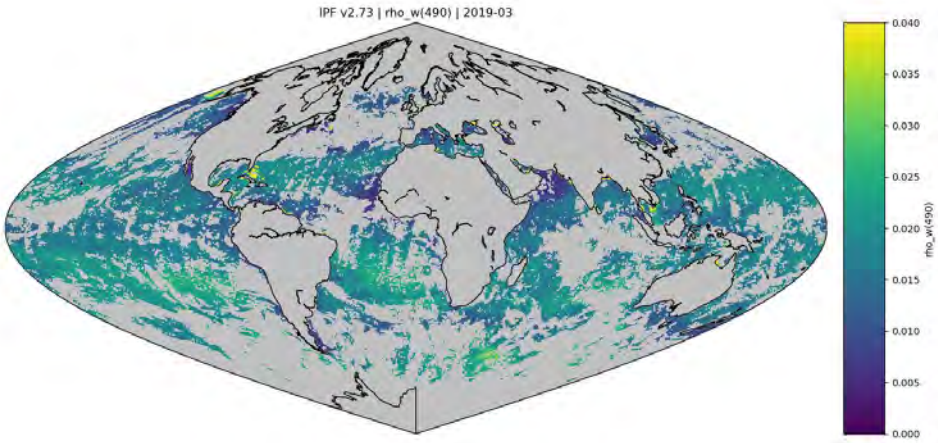

Figure 40: IPF v2.73 | rho_w(490) | 2019-03

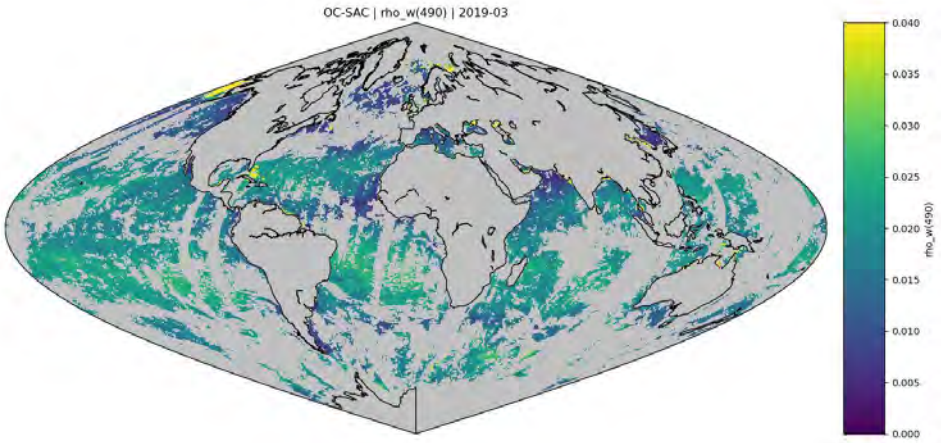

Figure 41: OC-SAC | rho_w(490) | 2019-03

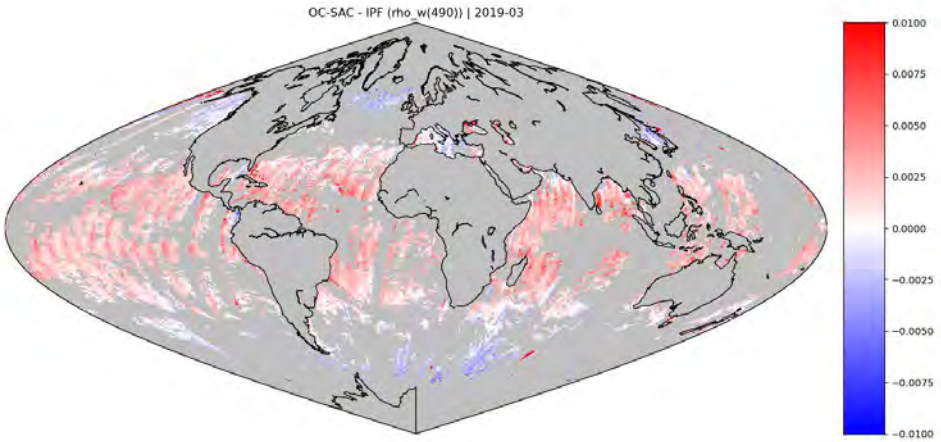

Figure 42: OC-SAC - IPF (rho_w(490)) | 2019-03

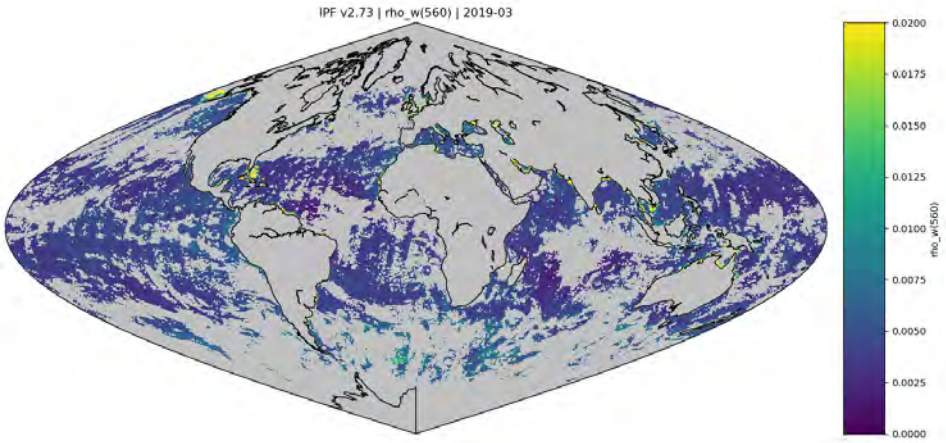

Figure 43: IPF v2.73 | rho_w(560) | 2019-03

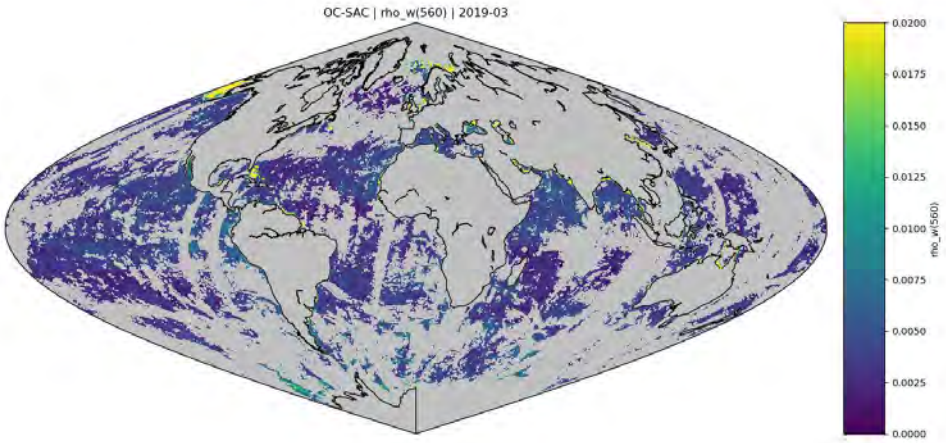

Figure 44: OC-SAC | rho_w(560) | 2019-03

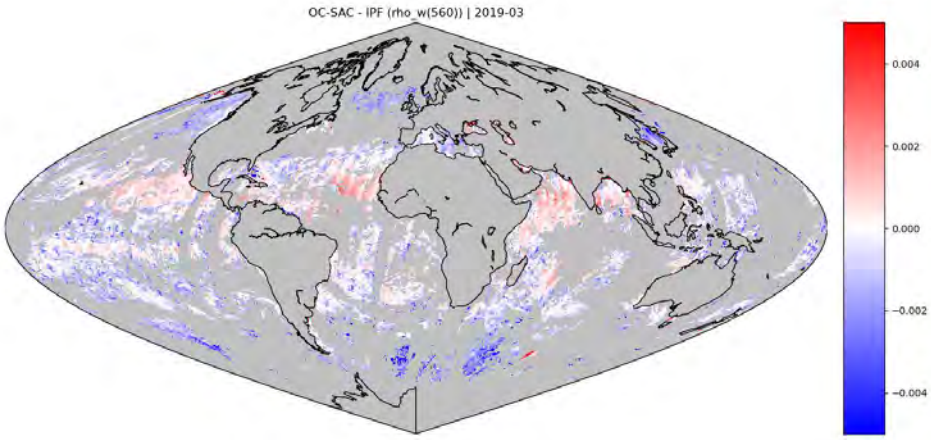

Figure 45: OC-SAC - IPF (rho_w(560)) | 2019-03

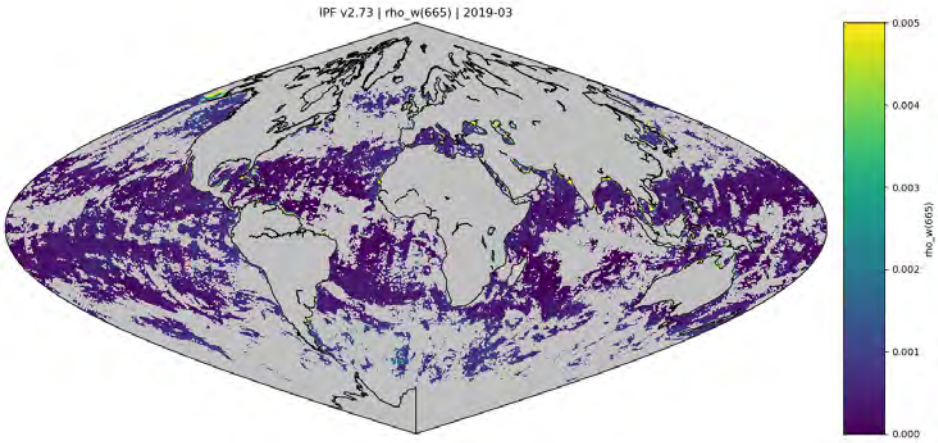

Figure 46: IPF v2.73 | rho_w(665) | 2019-03

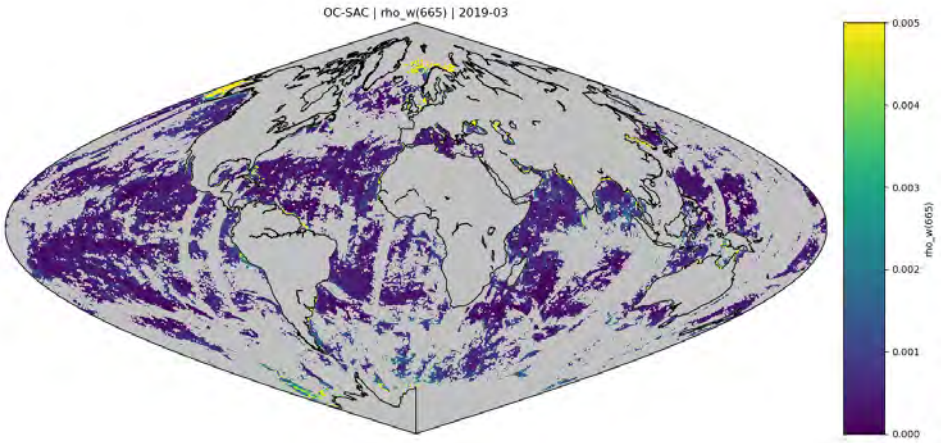

Figure 47: OC-SAC | rho_w(665) | 2019-03

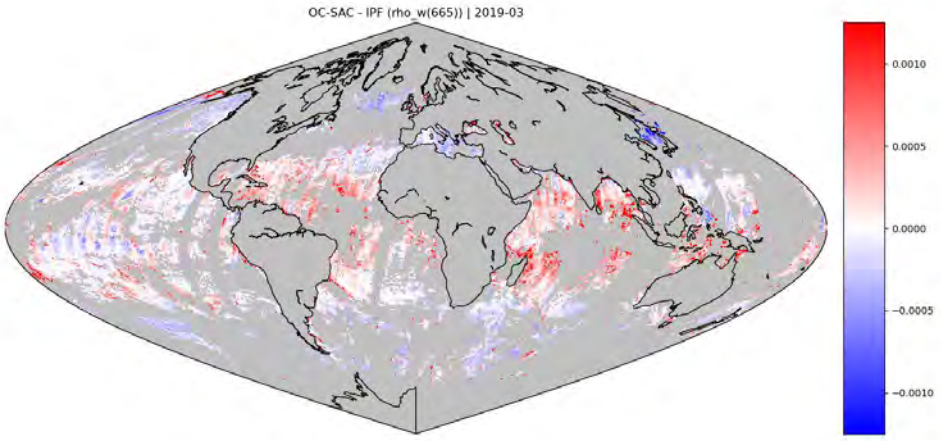

Figure 48: OC-SAC - IPF (rho_w(665)) | 2019-03

6 TIME SERIES ANALYSIS

6.1 METHOD

Time series are extracted over an area of 200x200 pixels of OLCI Reduced Resolution, centred at three locations:

Location	Coordinates	Map
South Pacific Gyre	24S, 122W	
Gulf of California	30.48N, 113.80W	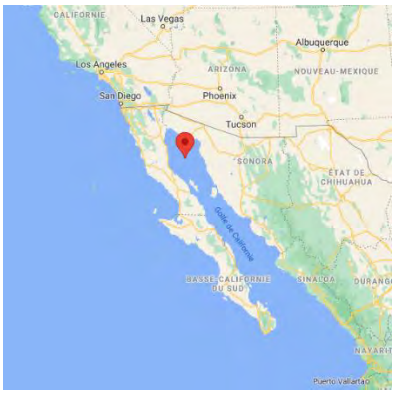
Arabian Sea	22.21N, 63.54E	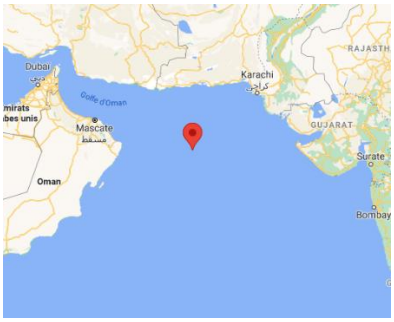

The mean value of the OC-SAC and IPF products are compared in the following section.

6.2 RESULTS

6.2.1 SPG

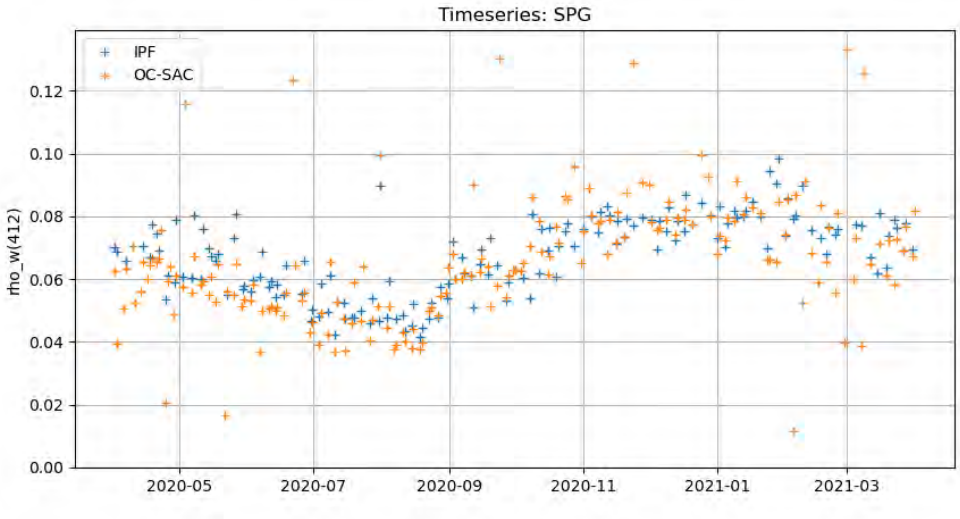

Figure 49: Timeseries of rho_w(412) [SPG]

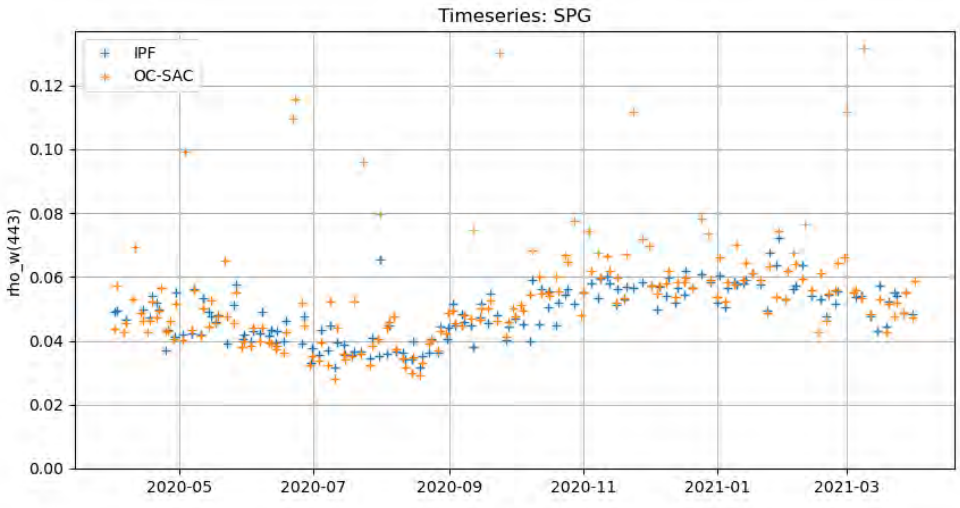

Figure 50: Timeseries of rho_w(443) [SPG]

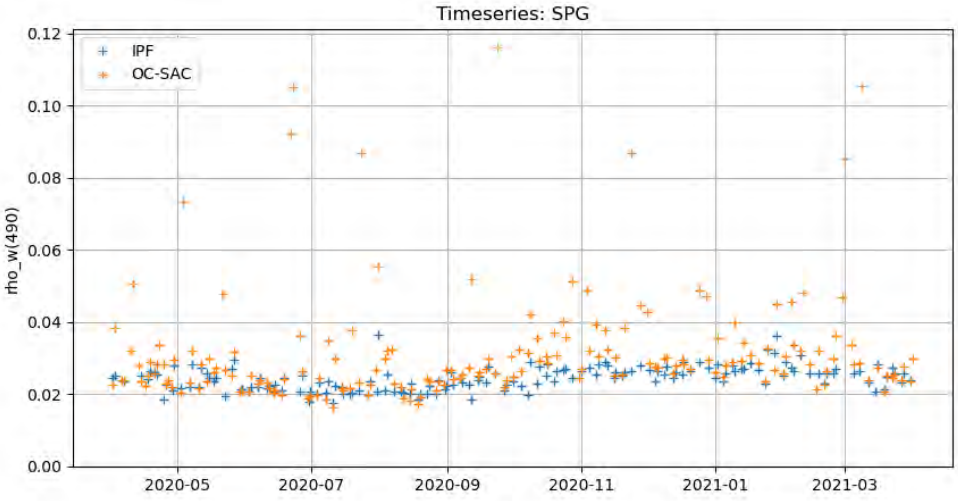

Figure 51: Timeseries of rho_w(490) [SPG]

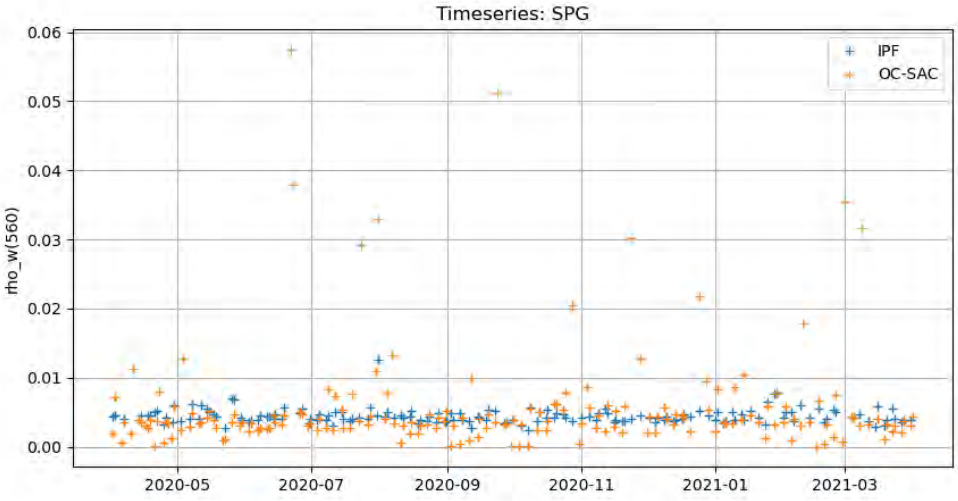

Figure 52: Timeseries of rho_w(560) [SPG]

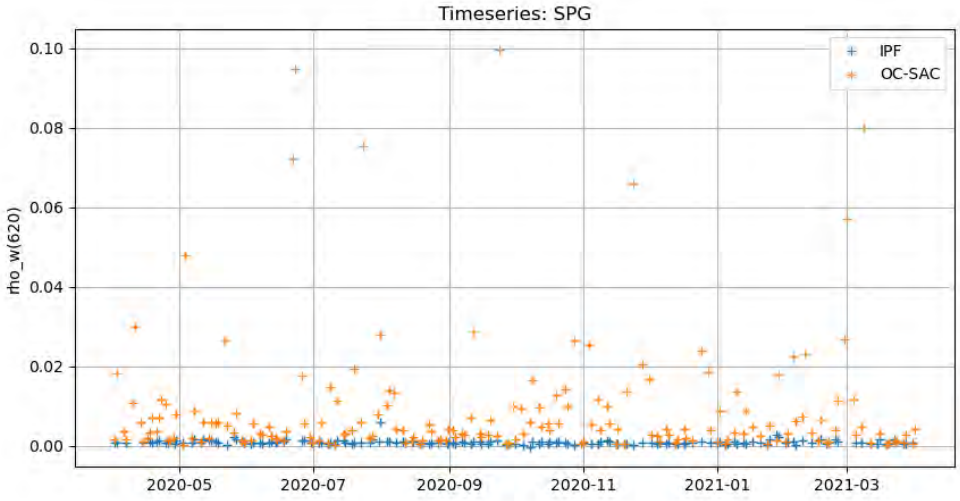

Figure 53: Timeseries of rho_w(620) [SPG]

6.2.2 GULF_CALIFORNIA

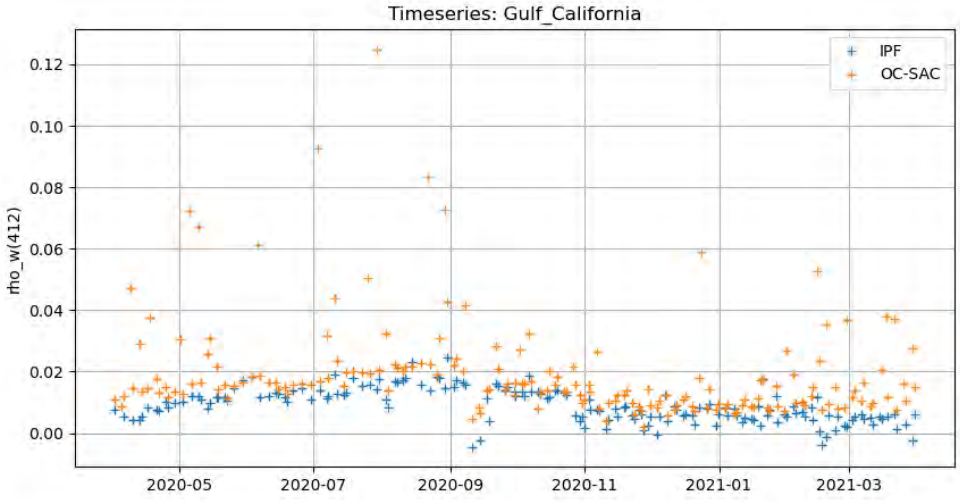

Figure 54: Timeseries of rho_w(412) [Gulf_California]

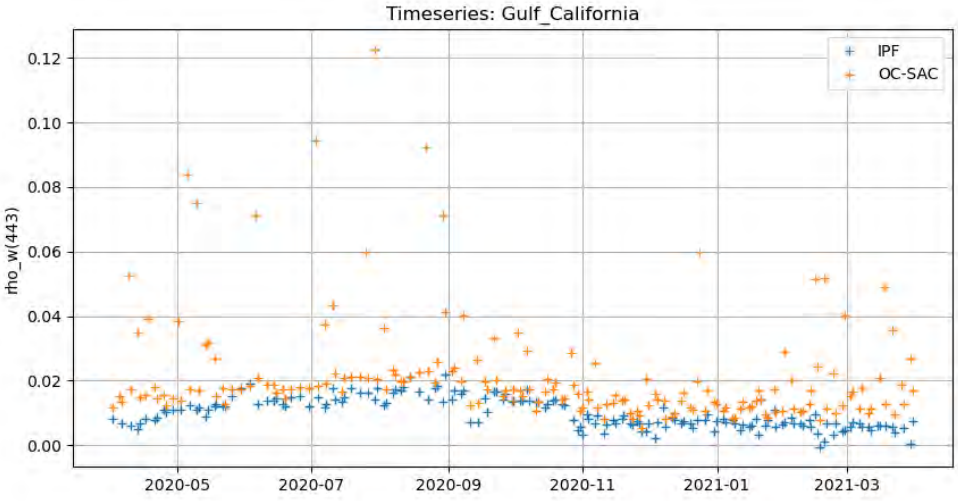

Figure 55: Timeseries of rho_w(443) [Gulf_California]

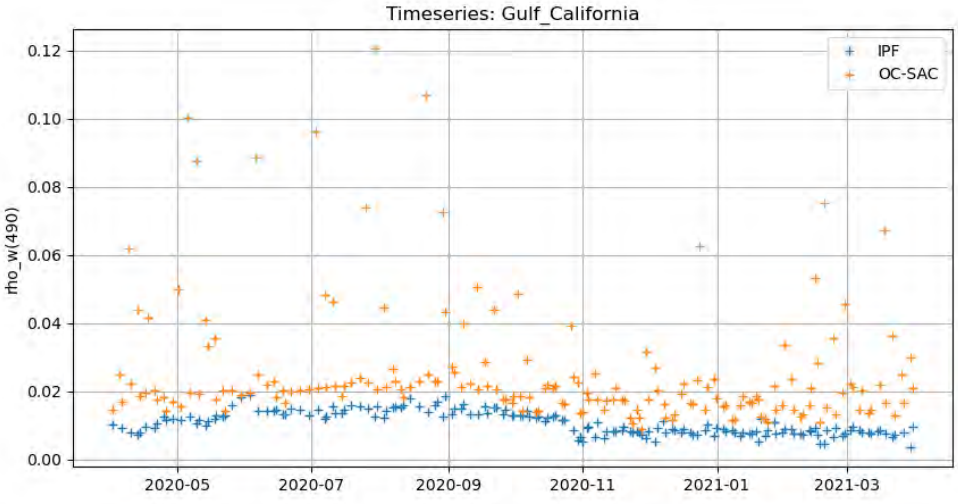

Figure 56: Timeseries of rho_w(490) [Gulf_California]

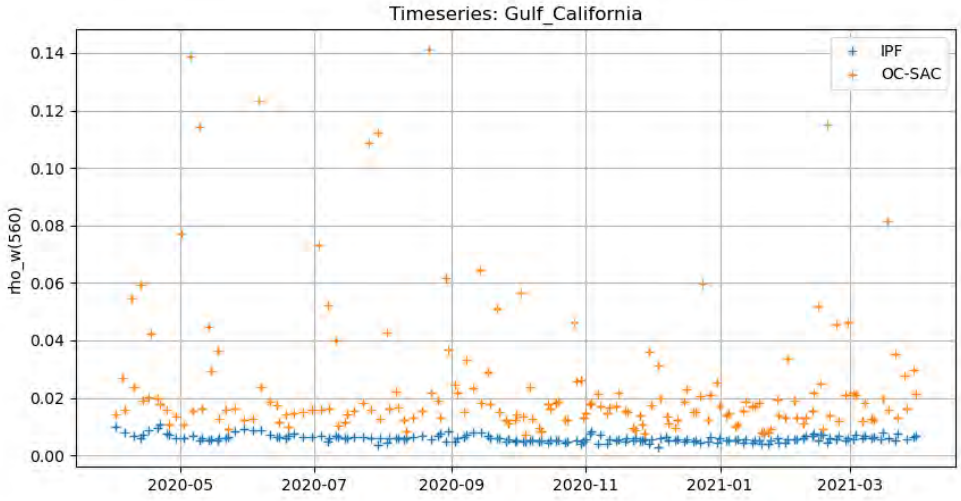

Figure 57: Timeseries of rho_w(560) [Gulf_California]

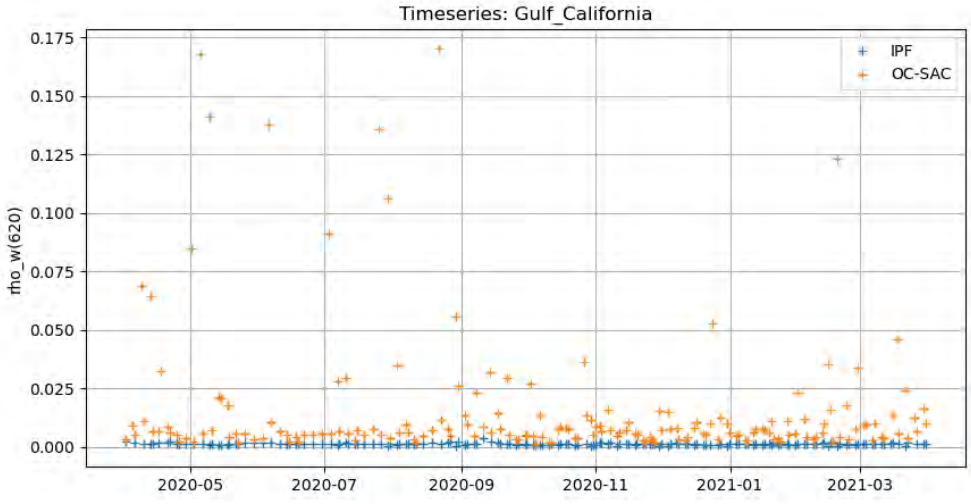

Figure 58: Timeseries of rho_w(620) [Gulf_California]

6.2.3 ARABIAN_SEA

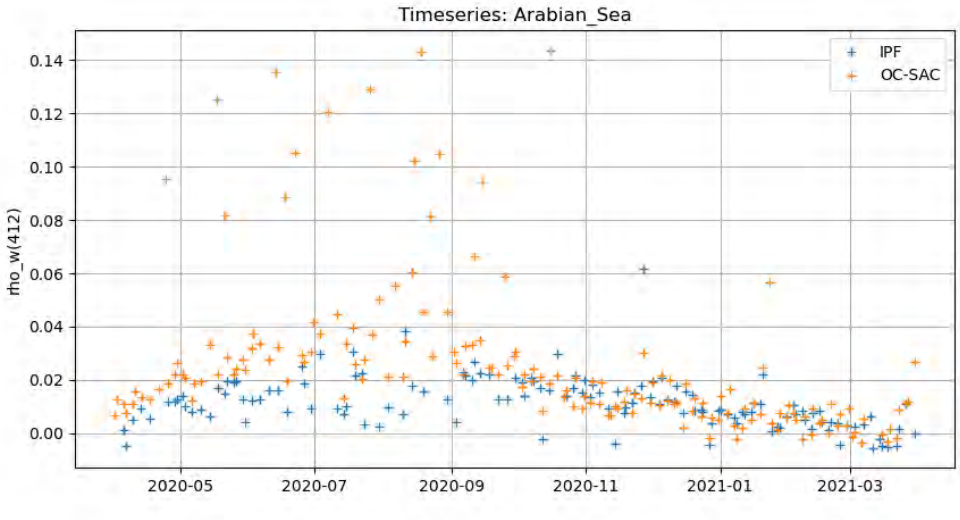

Figure 59: Timeseries of rho_w(412) [Arabian_Sea]

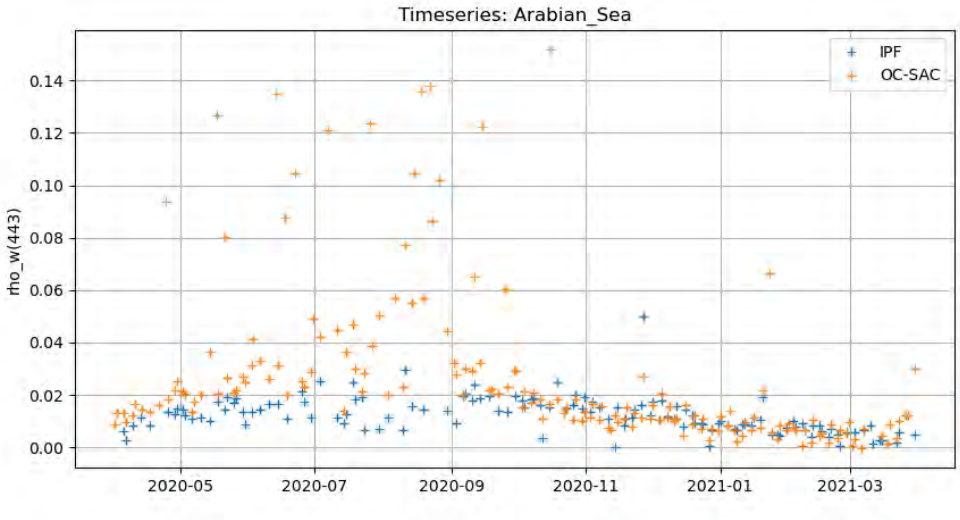

Figure 60: Timeseries of rho_w(443) [Arabian_Sea]

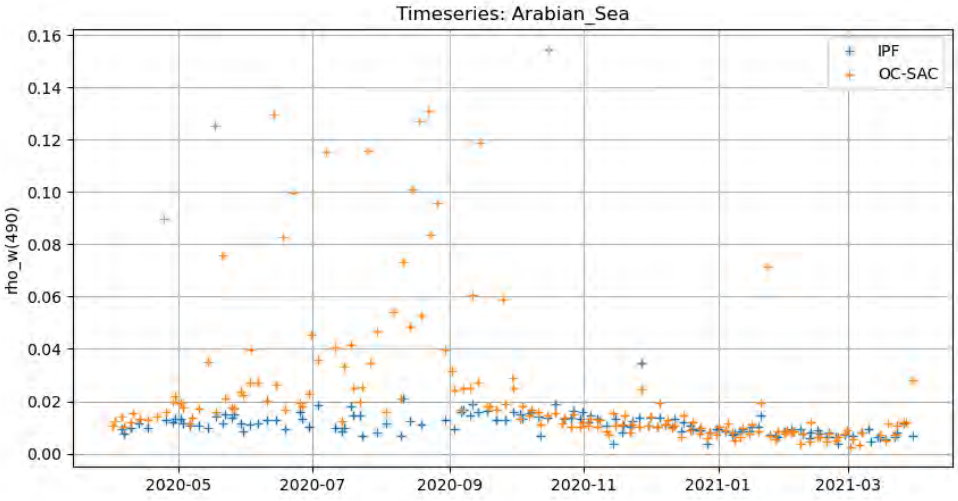

Figure 61: Timeseries of rho_w(490) [Arabian_Sea]

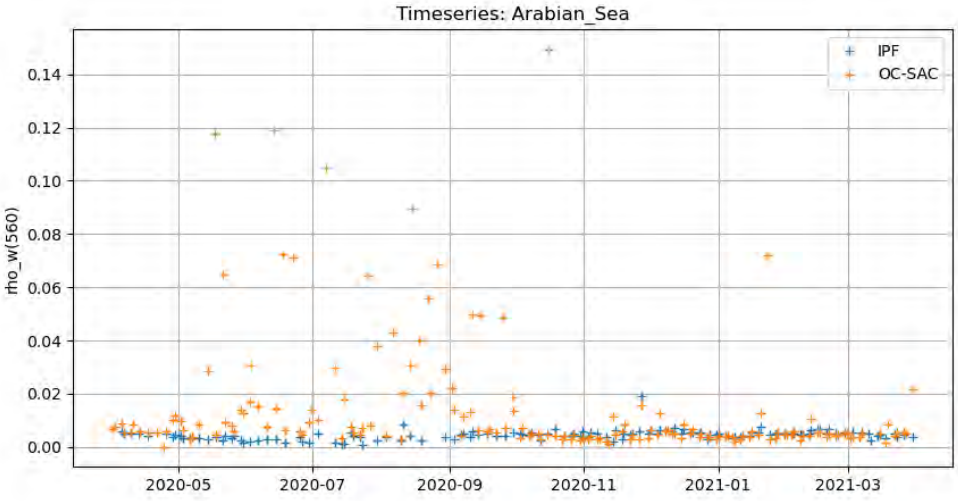

Figure 62: Timeseries of rho_w(560) [Arabian_Sea]

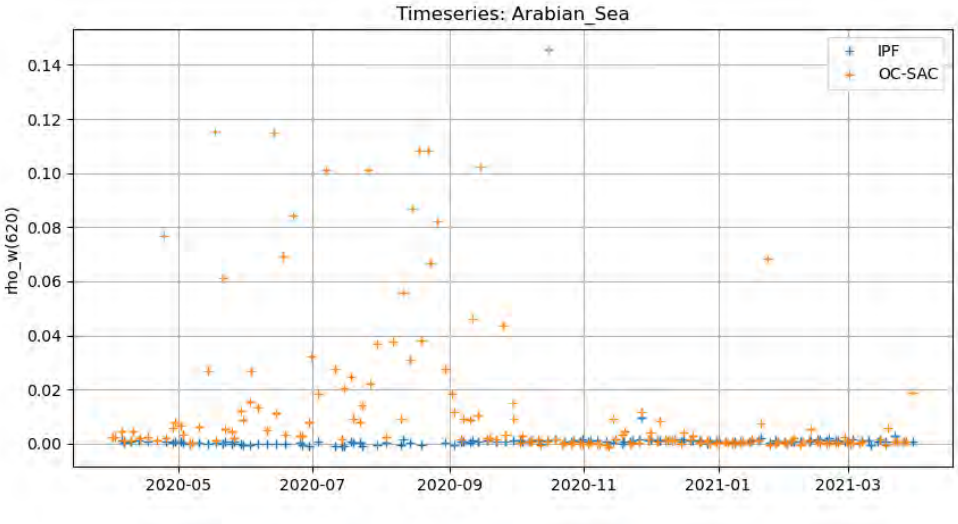

Figure 63: Timeseries of rho_w(620) [Arabian_Sea]

7 DISCUSSION

This analysis is preliminary because the OC-SAC flags are incomplete, in particular the CLOUD mask. However, this issue of alignment of the OC-SAC flags with those of the IPF concerns the OC-SAC prototype, not the module shared with the IPF. Other parts require consolidation, like the use of absorbing aerosols models.

Despite these issues and without any particular tuning of the OC-SAC module parameters, the results show good properties:

- **Validation** results show a slightly higher bias than IPF, but a **significantly reduced residual error** and Mean Absolute Deviation (sections 3.3.4to 3.3.6 with Common Best Quality).
- The processed scenes show an **improved ocean/atmosphere decorrelation**, like in 1-4_Coccolithophore_bloom (improved decorrelation is visible on the Angstrom coefficient)
- OC-SAC results show **less noise** than IPF, like in 1-8_Rio_de_la_Plata (visible on the AOT)
- Several scenes show **more homogeneous** data on OC-SAC, with fewer anomalous and flagged regions than the IPF. For example
    - On 1-3_North_Baltic_Sea (much less negative values in the Baltic)
    - On 3-1_Korea (more consistent results in the Yellow Sea, with much fewer flagged data)
    - On 3-2_Yangtse_Yellow_Sea (better rhow in the Yellow Sea, associated to lower AOT). OC-SAC seems **more robust than the IPF to the aerosol contamination**.
- In all scenes, OC-SAC presents **higher Angstrom** than IPF, what goes in the good direction (Angstrom of Collection 3 underestimated between -28% and -41% in Zibordi et al. 2022). Similarly, **AOT is generally higher**. Validation on AERONET data would have to be done to conclude on this improved performance.
- However, some suspect cases remain for OC-SAC, that need investigation:
    - 6-1_North_Sea: there is more invalid data with OC-SAC than IPF in the North Sea.
    - 6-3_Yellow_Sea: Angstrom coefficient obviously wrong and correlated with marine features in the Yangtse delta (for IPF too, but differently).

<u>Global difference maps</u>

The global difference maps (See section 4.2) show some interesting features. They show that **OC-SAC provides higher values than the IPF at low latitudes**, and **lower values at high latitudes**, especially in the blue bands. This is also seen at higher wavelengths, but to a lesser extent. In June and December (see Annex document), this feature drifts respectively to the North and South. We suspect that this bias between the two products could be linked with an anomaly previously observed on the IPF results, where a **positive bias increasing linearly with the air mass**, was emphasized by self-consistency analysis. At the level of individual scenes, this is also visible on 9-2_Svalbard, which is a scene at high latitude and high air mass. On this scene, we see on the water reflectance composite that OC-SAC provides lower reflectance in the blue bands, than the IPF.

These results confirm the usefulness of an additional investigation of this air mass dependency anomaly, which could not be carried out in this study.